Deployment of a Membrane Attached to Two Axially Moving Beams

Behrad Vatankhahghadim[1]
Institute for Aerospace Studies,
University of Toronto,
Toronto, ON M3H 5T6, Canada
e-mail: behrad.vatankhahghadim@mail.utoronto.ca

Christopher J. Damaren
Professor and Director
Institute for Aerospace Studies,
University of Toronto,
Toronto, ON M3H 5T6, Canada
e-mail: damaren@utias.utoronto.ca

The deployment dynamics of a simplified solar sail quadrant consisting of two Euler–Bernoulli beams and a flexible membrane are studied. Upon prescribing the in-plane motion and modeling the tension field based on linearly increasing stresses assumed on the attached boundaries, the coupled equations of motion that describe the system's transverse deflections are obtained. Based on these equations and their boundary conditions (BCs), deployment stability is studied by deriving simplified analytic expressions for the rate of change of system energy. It is shown that uniform extension and retraction result in decreasing and increasing energy, respectively. The motion equations are discretized using expansions in terms of "time-varying quasi-modes" (snapshots of the modes of a cantilevered beam and a clamped membrane), and the integrals needed for the resulting system matrices are rendered time-invariant via a coordinate transformation. Numerical simulation results are provided to illustrate a sample deployment and validate the analytic energy rate expressions. [DOI: 10.1115/1.4042134]

1 Introduction

Deployable membranes, such as solar sails and antenna reflectors, are finding an increasing number of applications in space structures, mainly because of their light weight and ability to be packaged efficiently. Studies conducted on deployment dynamics in the context of spacecraft can be traced back to 1960s, such as those reported in Refs. [1] and [2] on several large spin-stabilized space structures. The former considered radially telescoping and hinged deployment of inflexible booms, simplifying the study using point masses and disregarding any strain energies. The latter provided simulation results for a large paraboloid-shaped antenna (treated as a single massy spring) deployed using centrifugal forces. Deployment of flexible booms from spinning spacecraft was treated in Refs. [3] and [4]. Both works adopted a Lagrangian mechanics approach. The former simplified the analysis by neglecting the boom mass and studying the deployment of heavy concentrated tip masses, while the latter considered a long flexible boom and derived approximate solutions to the partial differential equations (PDEs) of motion using a time-varying quasi-modal approach (representing snapshots of the natural modes corresponding to the current length at each time). Lagrangian mechanics was also used in Refs. [5] and [6] to study the effects of extending rigid and flexible booms, respectively, on librational dynamics.

There is a rich body of literature on the general topic of axially translating media, such as strings and beams, with both fixed and variable lengths. Surveys of some of the early and more recent works (before 1970s and late 1980s) in such areas were presented in Refs. [7] and [8]. Studies of axially translating beams as a flexible deployment problem were performed in Refs. [9] and [10]. The choice of the coordinate system in Ref. [10] (which uses a similar motion equation to Ref. [9]) is not clear, but the reason [9] appears to be missing some gyroscopic terms in their equations of motion (according to Refs. [11] and [12]) is an error in the depiction of their coordinate system [13]. The stability results in Ref. [9] are, therefore, valid only in a moving coordinate system attached to the beam tip [13]. Discussions of the Eulerian (space-fixed) and Lagrangian (material-fixed) coordinate systems, and the equivalence of their ensuing results, were provided in Refs. [12] and [14].

Further studies on translating beam vibrations were performed in Refs. [15] and [16], primarily using Newtonian mechanics and variational principles, respectively; and in Ref. [17], treating time-varying extension rates and employing the extended Hamilton's principle. In all of these references, eigenfunctions of cantilevered beams were used as the time-varying basis functions for expressing transverse deflections. Justification of the time-varying quasi-modal approach and examination of its convergence to the generalized solution of the equations of motion were provided in Refs. [9] and [18]. In addition, a finite element method (FEM) formulation of and a stability study on an axially moving beam, using elements with time-varying length, were performed in Refs. [11] and [19], and the numerical results were compared against the experimental ones reported in Ref. [20]. Also using FEM, Refs. [21] and [22] focused on the dynamics of axially translating membranes, while Shin et al. [23] used the Galerkin method with admissible basis functions to discretize the equations of motion (an approach resembling that used in this manuscript). However, in the membrane studies in Refs. [21–23], one-dimensional (1D) motion along the fixed distance between two supports was considered, whereas this work focuses on time-varying length and deployment in two directions, as well as the beam–membrane coupling.

Returning to spacecraft applications and focusing on coupled systems, continuum mechanics-based approaches to deployment of large flexible solar arrays (with booms and blankets, such as those in the Communication Technology Satellite) were provided in Refs. [24–27], using quasi-modes with basis functions for both bending and twisting. Continuum mechanics and Rayleigh-Ritz approaches were also used in Refs. [28] and [29] for flexible dynamics and vibration characteristics of a boom-solar-panel system resembling that in the previous references. Although they assumed constant boom length and did not treat deployment, this work takes inspiration from their formulation of out-of-plane deflections in a manner that automatically guarantees compatibility of the two components' displacements at their points of attachment. A similar formulation (also using beam and string eigenfunctions) was used in Ref. [30] for coupled dynamics of a deploying boom-solar-panel. No stability study was provided, however, and in contrast to this work's inertial formulation, a moving coordinate system was used. Other spacecraft-related works include dynamics and stability of thin-walled shell structures, such as those in Refs. [31–33].

Focusing specifically on solar sails, the deployment dynamics of a simplified spinning model of IKAROS were studied in several resources, such as in Ref. [34], using the multiparticle model that assumes each finite element of the membrane is isotropic and

[1]Corresponding author.

Contributed by the Applied Mechanics Division of ASME for publication in the Journal of Applied Mechanics. Manuscript received September 12, 2018; final manuscript received November 28, 2018; published online December 24, 2018. Assoc. Editor: Ahmet S. Yigit.

replaced by particles (masses) connected by springs and dampers; and in Refs. [35] and [36], using the absolute nodal coordinate formulation (originally proposed in Ref. [37]) to reach a constant mass matrix by defining the location and deformation of all points in a global coordinate system. It is worth noting that, prior to IKAROS, the only successful case of deployment and control of spin-stabilized space structures was that of the Russian Znamya-2 in 1993 [38].

This document builds upon the past literature on axially translating media, and presents new results that are hoped to further the understanding of the deployment behavior of coupled beam–membrane systems (with solar sails used as a practical application). The aforementioned quasi-modal approach is adopted, mainly because of its computational efficiency compared to FEM [30]. In addition to modeling and simulation of the system's transient dynamics, vibration stability from an energy point of view is also considered in this work. Previous studies on the energetics of axially translating continua include those in Refs. [39–41], assuming constant length; and those in Refs. [17], [42], and [43], allowing for time-varying length. To the best of our knowledge, this work is a pioneering attempt in performing similar studies on coupled systems involving both second-order membrane-like and fourth-order beam-like components. For an alternative approach to deployment stability of translating continua based on boundedness of displacements, the reader is referred to Refs. [44–47]. In addition, although the present formulation is limited to a linearized study as an early attempt to tackle the coupled deployment dynamics problem, the authors recognize the importance of nonlinearities in thin and slender structures, and refer the interested reader to Refs. [22] and [48–50] for examples of nonlinear vibration studies on traveling strings, beams, and membranes; to Ref. [51–55] for nonlinear stability analyses of such continua (most of which feature time-varying translation speeds); and to Refs. [56] and [57] for surveys of nonlinear membrane vibration studies in general.

The organization of this manuscript is as follows: descriptions of the model and the simplifying assumptions made are provided in Sec. 2. Upon obtaining mathematical models of the velocity and stress fields within the system in Sec. 3, the governing equations of motion and their associated boundary conditions (BCs) are derived in Sec. 4. They are then used in Sec. 5 and discretized in Sec. 6 for the purposes of analytical stability analysis (in Sec. 5) and numerical simulations (in Sec. 7), respectively. Lastly, some concluding remarks are made in Sec. 8.

2 Model Description and Assumptions

For simplicity of exposition, most of the study presented in this paper is focused on only one sail quadrant that consists of a right triangular membrane attached continuously (at all points along its edges) to two booms. Recognizing that the complete (four-quadrant) sail dynamics will be different, allowing for both symmetric and antisymmetric modes, an extension of this document's formulation to a complete sail was provided in Ref. [47], along with additional simulation results.

The sail quadrant is modeled as a thin membrane with no bending stiffness and uniform density and thickness. The support booms are modeled as cantilevered Euler–Bernoulli beams with uniform density, cross-sectional area, and bending stiffness. They are assumed to have the same physical and geometric properties, and equal extension or retraction profiles with a constant velocity. In addition, as merely a starting point in this research direction, only small out-of-plane deformations, $w(x, y, t)$, are considered for all three components (as was also done in Refs. [11], [21], [23], and [46], among others), and the wrinkle/crease dynamics of the membrane are ignored. Based on the simulation results presented in Ref. [58] that accounts for both in-plane and out-of-plane deflections, the former (with length-normalized values in the order of 5×10^{-6} and 1×10^{-4} in the reported results) can be as much as two to four orders of magnitude smaller than the latter (in the order of 1×10^{-2} in the same simulations).

A sliding-type deployment is assumed, as shown in Fig. 1(*a*), during which the free edge of the membrane remains straight and at 45 deg to the booms. This assumption is reasonable only if the deployment rate is kept constant (which is the case in this problem), because otherwise a space-dependent inertial force distribution would develop within the membrane that could induce a curvature on the free edge. Moreover, the internal (inside the hub) portions of both booms and membrane are assumed to follow a fixed path to which no variation is applicable.

It is assumed that the membrane is under pretension provided by the support booms. A possible mechanism that could enable such a pretension may involve cables that run through the booms and are attached to the membrane quadrants from the excess parts that exit the boom tips. Pulling on the cables using an internally controlled mechanism would compress the boom and create a tension profile in the membrane. Such a mechanism would resemble that in Ref. [59], in which contraction of small cables that attach the membrane corners to the boom tips was used to control the membrane pretension. Of course, to avoid having to account for the cables in the model, their physical properties (such as mass) should be negligible compared to those of the membrane and the booms. For example, assuming cables of mass density 1440 kg/m^3 and semicircular cross-sectional radius 0.5 mm (both from Ref. [59]), a 10 m × 10 m sail would have cables of mass 0.01 kg (per quadrant) only, compared to 0.23 kg booms and 0.70 kg membrane (using mass densities of $\rho = 2.32 \times 10^{-2}$ kg/m and $\mu = 1.39 \times 10^{-2}$ kg/m^2, respectively, consistent with the values assumed later in Sec. 7.2).

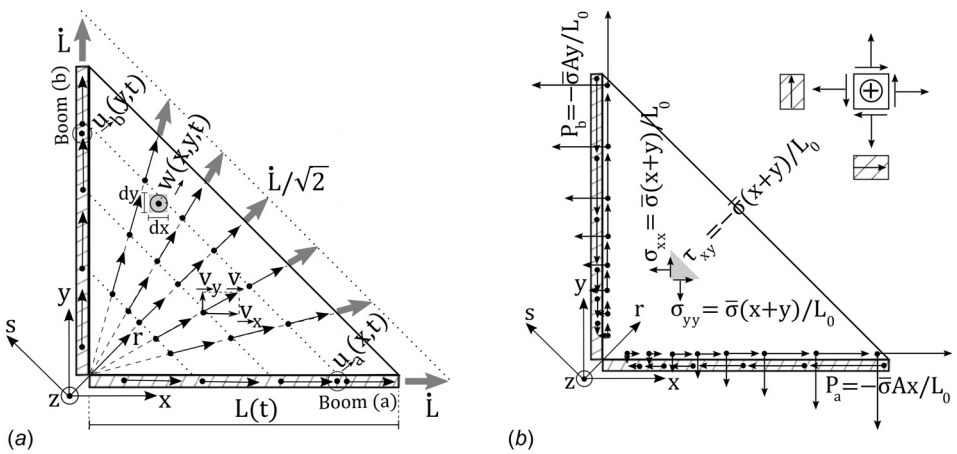

Fig. 1 Spatial distribution of (*a*) velocity field and (*b*) stress field

3 Velocity and Stress Fields

Based on the model and assumptions mentioned in Sec. 2, mathematical expressions are derived in Secs. 3.1 and 3.2 to describe the spatial distribution of the in-plane velocity and stress components pertinent to each mass element.

3.1 Velocity Field. A vector field that describes the in-plane deployment velocity of a differential mass element within the membrane or the booms, depending on the spatial position of the element, is required. Since no in-plane deflections are considered, this field is imposed by the booms' deployment rate. To this end, first the tilted (r, s) coordinate system in Fig. 1 is used, and the resulting vector field is then rotated back to the original (x, y) coordinate system. Consistent with the constant-rate sliding and straight free edge assumptions mentioned in Sec. 2, the axial (along the r-axis) component is taken to be $\dot{L}/\sqrt{2}$, and the transverse s-component is set to increase as one moves away from the diagonal. Using similar triangles, we have $v_r = \dot{L}/\sqrt{2}$ and $v_s = (s/r)v_r = (s/r)\dot{L}/\sqrt{2}$ as the r- and s-components of the mass elements' in-plane velocity. Using a 45 deg clockwise rotation about the z-axis normal to the membrane's neutral plane yields

$$v_x = \frac{\dot{L}}{2}\left(1+\frac{x-y}{x+y}\right), \quad v_y = \frac{\dot{L}}{2}\left(1-\frac{x-y}{x+y}\right) \tag{1}$$

where $v_x(x,y)$ and $v_y(x,y)$ are the x- and y-components of the mass elements' deployment velocity. A possible issue with this distribution is the singularity at the origin, $x=y=0$, which could be avoided by removing that single mass element from the model, hence rendering the system matrices finite as they should be. When needed, the mass element at (0,0) is considered to move along the diagonal with no transverse motion. The velocity field of Eq. (1) is depicted in Fig. 1(*a*).

3.2 Stress Field. A description of the stress field in the membrane and the booms is required for strain energy. To this end, the use of an Airy stress function, Φ, is proposed: a biharmonic function that, for plane stress and strain, satisfies [60]

$$\begin{gathered}\frac{\partial^4\Phi}{\partial x^4}+\frac{\partial^4\Phi}{\partial x^2\partial y^2}+\frac{\partial^4\Phi}{\partial y^4}=0\\ \sigma_{xx}=\frac{\partial^2\Phi}{\partial y^2}, \quad \sigma_{yy}=\frac{\partial^2\Phi}{\partial x^2}, \quad \tau_{xy}=\tau_{yx}=-\frac{\partial^2\Phi}{\partial x\partial y}\end{gathered} \tag{2}$$

where σ_{xx} and σ_{yy} are normal stresses, while $\tau_{xy}=\tau_{yx}$ are shear stresses. To obtain a suitable airy stress function, linearly increasing normal stresses on the two edges near the support booms (applied and maintained by the booms) and no stresses on the free edge are assumed, as shown in Fig. 1(*b*). The following stress function satisfies such boundary conditions:

$$\Phi = \left(\frac{\sigma}{6L}x^3+\frac{\sigma}{2L}x^2y\right)+\left(\frac{\sigma}{6L}y^3+\frac{\sigma}{2L}y^2x\right), \quad \sigma(t)\triangleq\bar{\sigma}\frac{L(t)}{L_0} \tag{3}$$

where $\bar{\sigma}$ is the initial (at time $t=0$) maximum tension value, experienced near the boom tips at (L_0, 0) and (0, L_0). The tip stress is assumed to temporally increase during extension and decrease during retraction. This is a reasonable assumption based on d'Alembert's principle, which generalizes the principle of virtual work to dynamics by introducing the notion of "force of inertia" [61]: the uniform outflow of mass during extension results in a constant increase in linear momentum, hence requiring increasing surface tractions (treated as external forces) to compensate for it. As a result of this assumption, the following force field (that remains spatially constant) is obtained using the relationships in Eq. (2):

$$N_{xx}=N_{yy}=-N_{xy}=\sigma_{xx}h=\bar{\sigma}h\frac{L}{L_0}\left(\frac{x}{L}+\frac{y}{L}\right) \tag{4}$$

where $N_{xx}(x,y)=N_{yy}(x,y)\triangleq\bar{N}(x,y)=(\bar{\sigma}h/L_0)(x+y)$ are normal forces per unit length, $N_{xy}(x,y)=N_{yx}(x,y)=-\bar{N}$ are shear forces per unit length, and h is the membrane's constant thickness. In addition, disregarding any inertial tension or compression forces caused by nonzero acceleration and given that the axial loads within the booms should balance out the boundary forces applied by the membrane, we have the following axial loads

$$\begin{aligned}P_a &= -\big(-\tau_{xy}(x,0)\big)A = -\frac{\bar{\sigma}A}{L_0}x,\\ P_b &= -\big(-\tau_{yx}(0,y)\big)A = -\frac{\bar{\sigma}A}{L_0}y\end{aligned} \tag{5}$$

where $P_a(x,t)$ and $P_b(y,t)$ are the axial loads on booms (a) and (b), respectively, and A is their constant cross-sectional area. It should be noted that the negative of the shear values are considered since positive shear is, by convention, defined in the opposite direction of the coordinate axes. If, for example, the membrane is in tension on one side, the corresponding boom will be in compression, similar to the solar panel tension and boom compression considered in Refs. [24], [25], and [30]. As a side note, accounting for time-varying deployment rate as part of future work would entail additional internal forces due to acceleration, such as $-\rho(L-x)\ddot{L}$ for boom (a).

4 Equations of Motion

This section summarizes the application of classical Lagrangian mechanics approaches to the problem of interest. Given the mass flow nature of the problem and the time-varying properties of the system, some remarks regarding the applicability of Hamilton's principle are in order and are thus provided in Sec 4.1. The system's Lagrangian and equations of motion are subsequently presented in Secs. 4.2 and 4.3 (with some derivation details saved for Appendix A).

4.1 Applicability of Hamilton's Principle. Hamilton's principle, in its classical form, was formulated for a system with a constant number of particles. When an Eulerian viewpoint (with its reference frame fixed to the spacecraft's hub) is adopted, the system of interest in this problem violates conservation of mass as additional portions of the booms and the membrane are extruded or retracted. To remedy the situation and justify the applicability of Hamilton's principle to this problem, two approaches previously used in the literature are readily applied to the two-dimensional (2D) coupled system of this paper: use of a sliding material-fixed reference frame as proposed in Ref. [16]; and use of a modified form of Hamilton's principle tailored to variable mass systems, developed in Ref. [62] (and subsequently used in Refs. [12] and [21] for beam deployment and axially moving membrane, respectively).

4.1.1 Lagrangian Viewpoint. Consider a material-fixed reference frame attached to the "root" of the membrane-boom system, hence sliding with them during deployment or retraction. Let the control system of interest include all parts of the booms and the membrane, including the portion still inside the hub, such that the number of particles is rendered constant, and the same particles are considered at all times. We can thus apply Hamilton's principle

$$\delta\int_{t_1}^{t_2}\mathscr{L}(x,y,t)\,dt=0 \Rightarrow \int_{t_1}^{t_2}\delta\iint_{S_{c,in}}\hat{\mathscr{L}}\,ds\,dt+\int_{t_1}^{t_2}\delta\iint_{S_{c,ex}}\hat{\mathscr{L}}^{0}\,ds\,dt=0 \tag{6}$$

where $\mathscr{L}$ and $\hat{\mathscr{L}}$ are the system's Lagrangian and its areal density, and $S_{c,in}$ and $S_{c,ex}$ are the projected areas (on the neutral plane) of

the portions of the closed control volume within and external to the hub, respectively. Assuming the parts inside the hub have a known configuration and follow an imposed path, their variation is set to zero, hence leaving only the Lagrangian of the materials' external portions to be considered.

4.1.2 Eulerian Viewpoint. Consider an open control volume around the combination of the booms and the membrane, a time-varying "window" in space that happens to enclose the booms' and the membrane's portions external to the hub. Let all surfaces of this control volume be closed, $B_c(t)$, except a small portion near the corner through which the components are deployed or retracted, $B_o(t)$ (later on, this entry point is idealized as only $(x, y) = (0, 0)$). Material transfer is permitted across this open surface, suggesting a need to recall a generalization, using Reynold's transport theorem and a moving open control volume, of Hamilton's principle to systems of time-varying mass [62]

$$\delta \int_{t_1}^{t_2} \mathscr{L}_o(x, y, t)\, dt + \int_{t_1}^{t_2} \int\int_{B_o(t)} \hat{m}(\underrightarrow{\boldsymbol{v}} \cdot \delta \underrightarrow{\boldsymbol{r}})(\underrightarrow{\boldsymbol{V}} - \underrightarrow{\boldsymbol{v}}) \cdot \underrightarrow{\hat{\boldsymbol{n}}}\, dS = 0 \tag{7}$$

where $\hat{m}$ is the mass density (ρ for the booms and μ for the membrane), $\underrightarrow{\hat{\boldsymbol{n}}}$ is the outward unit normal to the open control surface, and $\underrightarrow{\boldsymbol{v}}$ and $\underrightarrow{\boldsymbol{V}}$ are the material and control volume velocity vectors, respectively, at a point located in position $\underrightarrow{\boldsymbol{r}}$. The first integral in Eq. (7) relates to the variation of the Lagrangian within the control volume of interest (in this case, only the mass external to the hub), while the second term accounts for the momentum transfer associated with the mass flux through the open surface. As mentioned in Sec. 2, this manuscript accounts for transverse motion only (in contrast to the example of a flexible pipe with conveying fluid that was mentioned in Ref. [62]), hence not permitting any variations in the deployment direction. This implies $\delta \underrightarrow{\boldsymbol{r}} = \delta w \underrightarrow{\boldsymbol{z}}$. In addition, owing to the geometric BCs arising from the beams' cantilevered nature, the transverse displacements in the region of mass entry is prescribed as zero, resulting in $[\delta w = 0]_{B_o}$ and vanishing of the second term in Eq. (7). What remains is, therefore, the Lagrangian of the materials' external portion (within the open control volume).

4.2 System Lagrangian. The membrane's kinetic and strain energy, $\mathscr{T}_{\mathrm{M}}$ and $\mathscr{U}_{\mathrm{M}}$, based on Ref. [63] and ignoring terms higher than order one, are

$$\mathscr{T}_{\mathrm{M}} = \int_{0^+}^{L(t)} \int_{0^+}^{L(t)-x} \frac{1}{2}\left[\mu\left(v_{\mathrm{x}}^2 + v_{\mathrm{y}}^2\right) + \mu\left(\frac{\partial w}{\partial t} + v_{\mathrm{x}}\frac{\partial w}{\partial x} + v_{\mathrm{y}}\frac{\partial w}{\partial y}\right)^2\right] dy\, dx \tag{8a}$$

$$\mathscr{U}_{\mathrm{M}} = \int_{0^+}^{L(t)} \int_{0^+}^{L(t)-x} \frac{1}{2}\left[N_{\mathrm{xx}}\left(\frac{\partial w}{\partial x}\right)^2 + N_{\mathrm{yy}}\left(\frac{\partial w}{\partial y}\right)^2 + 2N_{\mathrm{xy}}\frac{\partial w}{\partial x}\frac{\partial w}{\partial y}\right] dy\, dx \tag{8b}$$

where $w(x, y, t)$ is the membrane's out-of-plane deflection, and μ is its uniform mass density. Analogously, the kinetic energy of boom (a) (along the x-axis), $\mathscr{T}_{\mathrm{B,a}}$, affected by both its translational and out-of-plane motions; and its strain potential energy, $\mathscr{U}_{\mathrm{B,a}}$, due to both its stiffness and axial loading from the membrane, are given by

$$\mathscr{T}_{\mathrm{B,a}} = \int_{0^+}^{L(t)} \frac{1}{2}\left[\rho\left(\dot{L}\underrightarrow{\boldsymbol{i}}_{\mathrm{x}} + 0\underrightarrow{\boldsymbol{i}}_{\mathrm{y}}\right) + \rho\left(\frac{\partial w}{\partial t} + \dot{L}\underrightarrow{\boldsymbol{i}}_{\mathrm{x}}\frac{\partial w}{\partial x} + 0\underrightarrow{\boldsymbol{i}}_{\mathrm{y}}\frac{\partial w}{\partial y}\right)^2\right]_{y=0} dx \tag{9a}$$

$$\mathscr{U}_{\mathrm{B,a}} = \int_{0^+}^{L(t)} \frac{1}{2}\left[EI\left(\frac{\partial^2 w}{\partial x^2}\right)^2 + P_{\mathrm{a}}\left(\frac{\partial w}{\partial x}\right)^2\right]_{y=0} dx \tag{9b}$$

where $w(x, 0, t) \triangleq u_{\mathrm{a}}(x, t)$ is the boom's out-of-plane deflection, and ρ is its uniform mass density. The intentional use of the same deflection variable as that of the membrane enforces the continuity of the two components' deflections along the edges (consistent with the assumption of continuous boom-membrane attachment). It is also recognized that $v_{\mathrm{x}}(x, 0, t) = \dot{L}$ and $v_{\mathrm{y}}(x, 0, t) = 0$ for purely horizontal deployment of boom (a). Combining the expressions in Eqs. (8) and (9), as well as those for boom (b) (similar to Eq. (9), but with x and y swapped), yields the total Lagrangian, $\mathscr{L} \triangleq (\mathscr{T}_{\mathrm{M}} - \mathscr{U}_{\mathrm{M}}) + (\mathscr{T}_{\mathrm{B,a}} - \mathscr{U}_{\mathrm{B,a}}) + (\mathscr{T}_{\mathrm{B,b}} - \mathscr{U}_{\mathrm{B,b}})$.

4.3 Governing Equations and Boundary Conditions. The system's governing equations and BCs can be derived by applying the extended Hamilton's principle (the use of which was justified in Sec. 4.1) and requiring the variation of the time integral (from t_0 to t_f) of the total Lagrangian in Sec. 4.2 to vanish. More details on the derivation are provided in Appendix A. Assuming constant deployment rate, the governing equations of the membrane, boom (a), and boom (b) are provided, in that order, by

$$\mu\left[\frac{\mathrm{D}^2 w}{\mathrm{D}t^2} + \underrightarrow{\nabla} \cdot \underrightarrow{\boldsymbol{v}}\frac{\mathrm{D}w}{\mathrm{D}t}\right] = \frac{\partial}{\partial x}(N_{\mathrm{xx}}w_{,x} + N_{\mathrm{xy}}w_{,y}) + \frac{\partial}{\partial y}(N_{\mathrm{xy}}w_{,x} + N_{\mathrm{yy}}w_{,y}) \tag{10a}$$

$$\left[\rho\frac{\mathrm{D}^2 w}{\mathrm{D}t^2} = (N_{\mathrm{yy}}w_{,y} + N_{\mathrm{xy}}w_{,x}) + \frac{\partial}{\partial x}(P_{\mathrm{a}}w_{,x}) - EIw_{,xxxx}\right]_{y=0} \tag{10b}$$

$$\left[\rho\frac{\mathrm{D}^2 w}{\mathrm{D}t^2} = (N_{\mathrm{xx}}w_{,x} + N_{\mathrm{xy}}w_{,y}) + \frac{\partial}{\partial y}(P_{\mathrm{b}}w_{,y}) - EIw_{,yyyy}\right]_{x=0} \tag{10c}$$

where $\underrightarrow{\nabla} \cdot \underrightarrow{\boldsymbol{v}} = v_{\mathrm{x},x} + v_{\mathrm{y},y}$ is the divergence of the velocity field provided by Eq. (1), and italicized subscripts after commas are introduced to represent spatial and temporal derivatives. The total derivatives (including convective terms) in Eq. (10) are given by $\mathrm{D}w/\mathrm{D}t \triangleq w_{,t} + v_{\mathrm{x}}w_{,x} + v_{\mathrm{y}}w_{,y}$ and $\mathrm{D}^2w/\mathrm{D}t^2 = \mathrm{D}(\mathrm{D}w/\mathrm{D}t)/\mathrm{D}t$.

It is noted that, in the case of the booms, the left-hand side of Eqs. (10*b*) and (10*c*) collapse down to the expressions provided in the past literature, such as in Ref. [16]: for example, for boom (a), we have $[\mathrm{D}^2w/\mathrm{D}t^2 = w_{,tt} + 2\dot{L}w_{,xt} + \dot{L}^2 w_{,xx}]_{y=0}$, the right-hand side terms of which relate to local, Coriolis, and centripetal accelerations, respectively [41,42]. As for the membrane, the right-hand side expression consists of $w_{,tt}$ for local acceleration, as well as $2(v_{\mathrm{x}}w_{,xt} + v_{\mathrm{y}}w_{,yt})$ and $v_{\mathrm{x}}^2 w_{,xx} + v_{\mathrm{y}}^2 w_{,yy} + 2v_{\mathrm{x}}v_{\mathrm{y}}w_{,xy}$ for two-dimensional versions of Coriolis and centripetal accelerations. If v_{y} is set to zero (one-dimensional deployment), the result in Eq. (10*a*) collapses down to the equation of motion in Ref. [21] for a membrane axially translating on two support rollers.

The natural BCs, that also arise from the variational approach of Appendix A, are provided below for the oblique free edge of the membrane and at the tips of booms (a) and (b), in that order:

$$[N_{\mathrm{xx}}w_{,x} + N_{\mathrm{yy}}w_{,y} + N_{\mathrm{xy}}(w_{,x} + w_{,y})]_{y=L-x} = 0 \tag{11a}$$

$$[w_{,xx}]_{(L,0)} = 0, \quad [EIw_{,xxx}]_{(L,0)} = [P_{\mathrm{a}}w_{,x}]_{(L,0)} \tag{11b}$$

$$[w_{,yy}]_{(0,L)} = 0, \quad [EIw_{,yyy}]_{(0,L)} = [P_{\mathrm{b}}w_{,y}]_{(0,L)} \tag{11c}$$

The conditions in Eqs. (11*b*) and (11*c*) require zero bending moment and shear (caused by the transverse components of both axial tension and flexural forces), while that in Eq. (11*a*) implies zero net transverse tensile force. Lastly, the geometric BCs imposed at the origin owing to the cantilevered nature assumed for the beams are $[w]_{(0,0)} = [w_{,x}]_{(0,0)} = [w_{,y}]_{(0,0)} = 0$. Note the coupling between the booms' and the membrane's dynamics: the governing equations of the booms, affected by the membrane's

dynamics (owing to the presence of $w_{,y}$ in Eq. (10*b*), for example) act as the along-the-boom BCs of the membrane. In addition, the N terms affect all governing equations and the tip BCs of the booms (via P).

5 Vibration Stability Analysis

The sign of the rate of change of vibration energy (disregarding the translational deployment motions) can be used as an indication of vibration stability from an energy viewpoint, as has been done in Refs. [9], [17], and [42]. For instance, strictly positive energy rate implies an incessant growth in vibration frequency. The vibration energy rate is denoted by $\dot{\mathscr{E}}_{\mathrm{v}} \triangleq \dot{\mathscr{E}}_{\mathrm{M,v}} + \dot{\mathscr{E}}_{\mathrm{B,a,v}} + \dot{\mathscr{E}}_{\mathrm{B,b,v}}$, with $\mathscr{E}_{\mathrm{M,v}} = \mathscr{T}_{\mathrm{M,v}} + \mathscr{U}_{\mathrm{M,v}}$ and so on. The integrands of $\mathscr{T}_{\mathrm{M,v}}$ and $\mathscr{T}_{\mathrm{B,a,v}}$ contain only the second terms in the integrands of Eqs. (8*a*) and (9*a*), while $\mathscr{U}_{\mathrm{M,v}}$ and $\mathscr{U}_{\mathrm{B,a,v}}$ are the same as those in Eqs. (8*b*) and (9*b*). The one- and two-dimensional versions of Leibniz's integral rule (stated and used in Appendix A) can be employed to write the energy rate constituents as

$$\begin{aligned}\dot{\mathscr{E}}_{\mathrm{M,v}} &= \int_{0^+}^{L}\int_{0^+}^{L-x} \mu\frac{\mathrm{D}w}{\mathrm{D}t}\left(w_{,tt}+\frac{\partial}{\partial t}(v_{\mathrm{x}}w_{,x})+\frac{\partial}{\partial t}(v_{\mathrm{y}}w_{,y})\right)dy\,dx \\ &+\int_{0^+}^{L}\int_{0^+}^{L-x}\left[N_{\mathrm{xx}}w_{,x}w_{,xt}+N_{\mathrm{yy}}w_{,y}w_{,yt}+N_{\mathrm{xy}}(w_{,xt}w_{,y}+w_{,x}w_{,yt})\right]dy\,dx \\ &+\frac{\dot{L}}{2}\int_{0^+}^{L}\left[\mu\left(\frac{\mathrm{D}w}{\mathrm{D}t}\right)^2+N_{\mathrm{xx}}w_{,x}^2+N_{\mathrm{yy}}w_{,y}^2+2N_{\mathrm{xy}}w_{,x}w_{,y}\right]_{y=L-x}dx\end{aligned} \tag{12a}$$

$$\begin{aligned}\dot{\mathscr{E}}_{\mathrm{B,a,v}} &= \int_{0^+}^{L}\left[\rho\frac{\mathrm{D}w}{\mathrm{D}t}\left(w_{,tt}+\frac{\partial}{\partial t}(v_{\mathrm{x}}w_{,x})\right)\right]_{y=0}dx \\ &+\int_{0^+}^{L}\left[EIw_{,xx}w_{,xxt}+P_{\mathrm{a}}w_{,x}w_{,xt}\right]_{y=0}dx \\ &+\frac{\dot{L}}{2}\left[\rho\left(\frac{\mathrm{D}w}{\mathrm{D}t}\right)^2+EIw_{,xx}^2+P_{\mathrm{a}}w_{,x}^2\right]_{(0,L)}\end{aligned} \tag{12b}$$

where $\dot{\mathscr{E}}_{\mathrm{M,v}}$ and $\dot{\mathscr{E}}_{\mathrm{B,a,v}}$ are the rates of change of vibration energy of the membrane and boom (a), respectively. A similar expression to Eq. (12*b*), but with x and y swapped, is applicable to $\dot{\mathscr{E}}_{\mathrm{B,b,v}}$ of boom (b).

As described in more detail in Appendix B, using the governing equations in Eq. (10), the natural and geometric BCs stated in Eq. (11) and its subsequent paragraph, and the fields in Eqs. (1) and (4) can ultimately simplify Eq. (12) to

$$\begin{aligned}\dot{\mathscr{E}}_{\mathrm{M,v}} &= -\frac{\mu\dot{L}}{2}\int_{0^+}^{L}\int_{0^+}^{L-x}\frac{1}{x+y}\left(\frac{\mathrm{D}w}{\mathrm{D}t}\right)^2dy\,dx \\ &-\int_{0^+}^{L}\left[\bar{N}\frac{\mathrm{D}w}{\mathrm{D}t}(w_{,x}-w_{,y})\right]_{x=0}dy-\int_{0^+}^{L}\left[\bar{N}\frac{\mathrm{D}w}{\mathrm{D}t}(w_{,y}-w_{,x})\right]_{y=0}dx\end{aligned} \tag{13a}$$

$$\begin{aligned}\dot{\mathscr{E}}_{\mathrm{B,a,v}} &= -\frac{EI\dot{L}}{2}\left[w_{,xx}^2\right]_{(0,0)}+\frac{\dot{L}}{2}\int_{0^+}^{L}\left[P_{\mathrm{a},x}w_{,x}^2\right]_{y=0}dx \\ &+\int_{0^+}^{L}\left[\bar{N}\frac{\mathrm{D}w}{\mathrm{D}t}(w_{,y}-w_{,x})\right]_{y=0}dx\end{aligned} \tag{13b}$$

Upon adding the results, it is observed that the last term in Eq. (13*b*) and that of the analogous expression for boom (b) cancel out the second and third terms in Eq. (13*a*). Lastly, after substituting $P_{\mathrm{a},x} = P_{\mathrm{b},y} = -\bar{\sigma}A/L_0$ based on Eq. (5), we have

$$\begin{aligned}\dot{\mathscr{E}}_{\mathrm{v}} &= -\frac{\dot{L}}{2}\left[\mu\int_{0^+}^{L}\int_{0^+}^{L-x}\frac{1}{x+y}\left(\frac{\mathrm{D}w}{\mathrm{D}t}\right)^2dy\,dx+EI\left[w_{,xx}^2+w_{,yy}^2\right]_{(0,0)}\right. \\ &\left.+\frac{\bar{\sigma}A}{L_0}\int_{0^+}^{L}\left[w_{,x}^2\right]_{y=0}dx+\frac{\bar{\sigma}A}{L_0}\int_{0^+}^{L}\left[w_{,y}^2\right]_{x=0}dy\right]\end{aligned} \tag{14}$$

Since all the terms inside the brackets are non-negative, the conclusion is that for constant-rate deployment of a coupled boom-membrane system with the velocity and stress fields assumed in this paper, $\dot{\mathscr{E}}_{\mathrm{v}} \le 0$ for $\dot{L} > 0$ (extension), implying "vibration stability" associated with ever-decreasing vibration energy; whereas $\dot{\mathscr{E}}_{\mathrm{v}} \ge 0$ for $\dot{L} < 0$ (retraction), suggesting "vibration instability." This result collapses down to one consistent with Ref. [17] for a beam-only deployment problem. It is noted, however, that boundedness of vibration energy does not necessarily imply that of displacements [45]. The deployment stability of a complete sail from a displacement viewpoint and using the system's eigenvalues is examined in Ref. [47].

6 Descretized Equations of Motion

This section describes the discretization approach used on the equations of motions in Sec. 4 to make them suitable for numerical integration. Section 6.1 explains how deflections are expanded in terms of time-varying modes, Secs. 6.2 and 6.3 present the system matrices and their modification based on a coordinate transformation, and Sec. 6.4 concludes the discussion by providing the discretized equations of motion.

6.1 Quasi-Modal Expansion. The quasi-modal approach with time-varying mode shapes used in Refs. [3], [17], and [27], among others, is adopted, where the well-known eigenfunctions of beams, but using time-varying length, were employed. The following quasi-modal expansions are introduced for the out-of-plane deflections of boom (a), boom (b), and the membrane, in that order

$$u_{\mathrm{a}}(x,t) = \sum_{k=1}^{\infty} p_{\mathrm{a}_k}(t)\psi_{\mathrm{a}_k}(x,t) = \boldsymbol{p}_{\mathrm{a}}^{\top}(t)\boldsymbol{\Psi}_{\mathrm{a}}(x,t) \tag{15a}$$

$$u_{\mathrm{b}}(y,t) = \sum_{k=1}^{\infty} p_{\mathrm{b}_k}(t)\psi_{\mathrm{b}_k}(y,t) = \boldsymbol{p}_{\mathrm{b}}^{\top}(t)\boldsymbol{\Psi}_{\mathrm{b}}(y,t) \tag{15b}$$

$$\begin{aligned}w(x,y,t) &= u_{\mathrm{a}}(x,t)+u_{\mathrm{b}}(y,t)+\sum_{k=1}^{\infty}q_k(t)\phi_k(x,y,t) \\ &= u_{\mathrm{a}}+u_{\mathrm{b}}+\boldsymbol{q}^{\top}(t)\boldsymbol{\Phi}(x,y,t)\end{aligned} \tag{15c}$$

It is noted that the membrane deflections are taken to consist of the superimposition of that of a membrane clamped at the edges on those of the support booms. The basis functions used in the expansions are taken to be the eigenfunctions of a cantilevered beam and a (rectangular) clamped membrane

$$\psi_k = \cos\left(\beta_k\frac{x}{L}\right)-\cosh\left(\beta_k\frac{x}{L}\right)-\kappa_k\left[\sin\left(\beta_k\frac{x}{L}\right)-\sinh\left(\beta_k\frac{x}{L}\right)\right] \tag{16a}$$

$$\phi_k = \sin\left(i\pi\frac{x}{L}\right)\sin\left(j\pi\frac{y}{L}\right) \tag{16b}$$

where $\{i,j\} \in \{1,2,\ldots,\sqrt{n_{\mathrm{M}}}\}$ are ordered pairs of coefficients corresponding to the kth mode out of a total of n_{M} membrane modes. The variables β_k are solutions of $\cos(\beta_k)\cosh(\beta_k)+1=0$, a list of which can be found in Ref. [64]. The constant coefficients in Eq. (16*a*) are given by $\kappa_k \triangleq (\cos(\beta_k)+\cosh(\beta_k))/(\sin(\beta_k)+\sinh(\beta_k))$. The time dependence of the mode shapes arises from

the fact that $L(t)$ varies as the boom extends and the membrane is deployed. As an aside, the reader should note that, even though the basis functions in Eq. (16*b*) correspond to the eigenfunctions of a rectangular membrane, they are still complete and compatible with the boundary conditions, and hence sufficient for the purposes of the Ritz-type discretization used in this section [65].

6.2 System Matrices. Finite numbers of modes, n_B and n_M for the booms and the membrane, respectively, are considered. Upon substituting the truncated forms of the expansion in Eq. (15*a*) into Eq. (9), the Lagrangian of boom (a) takes the form

$$\mathscr{L}_{B,a} = \frac{1}{2}\rho L\dot{L}^2 + \frac{1}{2}\dot{\boldsymbol{p}}_a^\top \boldsymbol{M}_B \dot{\boldsymbol{p}}_a + \dot{\boldsymbol{p}}_a^\top \boldsymbol{G}_B \boldsymbol{p}_a + \frac{1}{2}\boldsymbol{p}_a^\top (\boldsymbol{K}_{B,T} - \boldsymbol{K}_{B,U})\boldsymbol{p}_a \tag{17}$$

where the matrices are defined as

$$\boldsymbol{M}_B \triangleq \int_{0^+}^{L} \rho \boldsymbol{\Psi}_a \boldsymbol{\Psi}_a^\top \, dx \tag{18a}$$

$$\boldsymbol{G}_B \triangleq \int_{0^+}^{L} \rho\left(v_x - \frac{\dot{L}}{L}x\right)\boldsymbol{\Psi}_a \boldsymbol{\Psi}_{a,x}^\top \, dx \tag{18b}$$

$$\boldsymbol{K}_{B,T} \triangleq \int_{0^+}^{L} \rho\left(v_x - \frac{\dot{L}}{L}x\right)^2 \boldsymbol{\Psi}_{a,x} \boldsymbol{\Psi}_{a,x}^\top \, dx \tag{18c}$$

$$\boldsymbol{K}_{B,U} \triangleq \int_{0^+}^{L} (P_a \boldsymbol{\Psi}_{a,x} \boldsymbol{\Psi}_{a,x}^\top + EI \boldsymbol{\Psi}_{a,xx} \boldsymbol{\Psi}_{a,xx}^\top) \, dx \tag{18d}$$

where $v_x = \dot{L}$ in this case, $\boldsymbol{\Psi}_a(x,t)$ is the column matrix of beam eigenfunctions defined in Eq. (16*a*), and $\boldsymbol{\Psi}_{a,x}(x,t)$ and $\boldsymbol{\Psi}_{a,xx}(x,t)$ are its first- and second-order spatial derivatives, respectively. The same expressions, but with x replaced by y, hold for boom (b), but the resulting matrices will be the same for identical booms if equal deployment rates are assumed. Lastly, it should be noted that all of these matrices can be evaluated analytically. For example, Eq. (18*a*) and the second part of Eq. (18*d*) yield $\boldsymbol{M}_B = \text{diag}\{\rho L\}$ and $\boldsymbol{K}_{B,U,2} = \text{diag}\{EI(\beta_k^4/L^3)\}$ for $k \in \{1, \ldots, n_B\}$ [64].

Similarly, shifting the focus to the membrane, upon substituting the truncated form of Eq. (15*c*) into Eq. (8), the Lagrangian of the membrane is obtained in discretized form

$$\mathscr{L}_M = \frac{\mu}{2}\int_{0^+}^{L}\int_{0^+}^{L-x}\left(v_x^2 + v_y^2\right) dy\, dx + \frac{1}{2}\dot{\tilde{\boldsymbol{q}}}^\top \tilde{\boldsymbol{M}}_M \dot{\tilde{\boldsymbol{q}}} + \dot{\tilde{\boldsymbol{q}}}^\top \tilde{\boldsymbol{G}}_M \tilde{\boldsymbol{q}} + \frac{1}{2}\tilde{\boldsymbol{q}}^\top (\tilde{\boldsymbol{K}}_{M,T} - \tilde{\boldsymbol{K}}_{M,U})\tilde{\boldsymbol{q}} \tag{19}$$

where the tilde sign over the matrices indicates "augmented" variables of size $n \times 1$ or $n \times n$, with $n = n_M + 2n_B$ being the total number of system modes. For example, $\tilde{\boldsymbol{q}} \triangleq [\boldsymbol{p}_a^\top \; \boldsymbol{p}_b^\top \; \boldsymbol{q}^\top]^\top$ consists of all of the system's generalized coordinates. The augmented matrices are defined as

$$\tilde{\boldsymbol{M}}_M \triangleq \int_{0^+}^{L}\int_{0^+}^{L-x} \mu \tilde{\boldsymbol{A}}\tilde{\boldsymbol{A}}^\top \, dy\, dx \tag{20a}$$

$$\tilde{\boldsymbol{G}}_M \triangleq \int_{0^+}^{L}\int_{0^+}^{L-x} \mu \tilde{\boldsymbol{A}}\tilde{\boldsymbol{B}}^\top \, dy\, dx \tag{20b}$$

$$\tilde{\boldsymbol{K}}_{M,T} \triangleq \int_{0^+}^{L}\int_{0^+}^{L-x} \mu \tilde{\boldsymbol{B}}\tilde{\boldsymbol{B}}^\top \, dy\, dx \tag{20c}$$

$$\tilde{\boldsymbol{K}}_{M,U} \triangleq \int_{0^+}^{L}\int_{0^+}^{L-x} (N_{xx}\tilde{\boldsymbol{C}}\tilde{\boldsymbol{C}}^\top + N_{yy}\tilde{\boldsymbol{D}}\tilde{\boldsymbol{D}}^\top + N_{xy}(\tilde{\boldsymbol{C}}\tilde{\boldsymbol{D}}^\top + \tilde{\boldsymbol{D}}\tilde{\boldsymbol{C}}^\top)) \, dy\, dx \tag{20d}$$

for which the following matrices, consisting of both boom and membrane eigenfunctions and their derivatives, are used:

$$\tilde{\boldsymbol{A}} \triangleq \begin{bmatrix} \boldsymbol{\Psi}_a \\ \boldsymbol{\Psi}_b \\ \boldsymbol{\Phi} \end{bmatrix}, \; \tilde{\boldsymbol{C}} \triangleq \begin{bmatrix} \boldsymbol{\Psi}_{a,x} \\ \boldsymbol{0} \\ \boldsymbol{\Phi}_{,x} \end{bmatrix}, \; \tilde{\boldsymbol{D}} \triangleq \begin{bmatrix} \boldsymbol{0} \\ \boldsymbol{\Psi}_{b,y} \\ \boldsymbol{\Phi}_{,y} \end{bmatrix},$$
$$\tilde{\boldsymbol{B}} \triangleq \left(v_x - \frac{\dot{L}}{L}x\right)\tilde{\boldsymbol{C}} + \left(v_y - \frac{\dot{L}}{L}y\right)\tilde{\boldsymbol{D}}$$

where $\boldsymbol{\Psi}_a(x,t)$, $\boldsymbol{\Psi}_b(y,t)$, and $\boldsymbol{\Phi}(x,y,t)$ are the column matrices of the beam and membrane basis functions defined in Eqs. (15*a*)–(15*c*), respectively; and $\boldsymbol{\Psi}_{a,x}$, $\boldsymbol{\Psi}_{b,y}$, $\boldsymbol{\Phi}_{,x}$, and $\boldsymbol{\Phi}_{,y}$ are their first-order spatial derivatives.

6.3 Transformed System Matrices. The matrices obtained in Sec. 6.2 to express the system Lagrangian can be converted to a form involving time-independent matrices by transforming the problem from that of spatially fixed points within time-varying boundaries, namely x and y that satisfy $0 < x < L(t)$ and $0 < y < L(t)$, to that of moving points within fixed boundaries, namely $\hat{x} \triangleq x/L(t)$ and $\hat{y} \triangleq y/L(t)$ that satisfy $0 < \hat{x}(t) < 1$ and $0 < \hat{y}(t) < 1$. The use of this transformation in the context of axially translating media and spinning deployment can be traced back to Refs. [10] and [26], respectively, and is also seen in Refs. [20], [30], and [50]. Very significant computational cost-saving results from this approach. For example, a MATLAB simulation run that would originally last about 24 h using two 3.40 GHz CPUs was reduced to only about 6 min thanks to this transformation.

To adopt such a transformation, the space- and time-derivatives of all variables should be modified as follows:

$$\frac{\partial}{\partial x}(\cdot) = \frac{1}{L}\frac{\partial}{\partial \hat{x}}(\cdot), \;\; \frac{\partial^2}{\partial x^2}(\cdot) = \frac{1}{L^2}\frac{\partial^2}{\partial \hat{x}^2}(\cdot), \;\; \frac{\partial^2}{\partial x \partial y}(\cdot) = \frac{1}{L^2}\frac{\partial^2}{\partial \hat{x}\partial \hat{y}}(\cdot),$$
$$\frac{\partial}{\partial t}(\cdot)\Big|_{(x,y)} = \frac{\partial}{\partial t}(\cdot)\Big|_{(\hat{x},\hat{y})} - \frac{\hat{x}\dot{L}}{L}\frac{\partial}{\partial \hat{x}}(\cdot)\Big|_{(\hat{x},\hat{y})} - \frac{\hat{y}\dot{L}}{L}\frac{\partial}{\partial \hat{y}}(\cdot)\Big|_{(\hat{x},\hat{y})} \tag{21}$$

with expressions analogous to the first two for $\partial/\partial y(\cdot)$ and $\partial^2/\partial y^2(\cdot)$. The right-hand side of the last expression in Eq. (21) accounts for both local time variations and the convective terms owing to the motion of the $\hat{x}$ and $\hat{y}$ coordinates. The velocity and stress distributions in Secs. (3.1) and (3.2) are rewritten in terms of $\hat{x}$ and $\hat{y}$, for example, $N_{xx} = \bar{\sigma}hL/L_0(\hat{x} + \hat{y})$; so are the derivatives of the eigenfunction matrices, for example, $\boldsymbol{\Psi}_{a,x}(x) = \boldsymbol{\Psi}_{a,\hat{x}}(\hat{x})/L$ (based on Eq. (21)). With these transformations and upon extracting L and $\dot{L}$ out of the integrals in Eqs. (18) and (20), their integrands become $\hat{x}$- and/or $\hat{y}-$ dependent but time-independent, for example, $\boldsymbol{M}_B = \rho L \int_{0^+}^{1} \boldsymbol{\Psi}_a \boldsymbol{\Psi}_a^\top \, d\hat{x}$. As a result, numerical integration (in the absence of analytic expressions) is only required to be performed once, and not at each time-step.

6.4 Euler–Lagrange Equations. Having determined the Lagrangian of boom (a) in Eq. (17) and that of the membrane in Eq. (19), the total system Lagrangian for the membrane quadrant of interest is obtained by their addition (together with that of boom (b)). Upon using the classical Euler–Lagrange formulation, the following discretized equations of motion are arrived at:

$$[\tilde{\boldsymbol{M}}_M + \tilde{\boldsymbol{M}}_B]\ddot{\tilde{\boldsymbol{q}}} + [(\dot{\tilde{\boldsymbol{M}}}_M + \dot{\tilde{\boldsymbol{M}}}_B) + (\tilde{\boldsymbol{G}}_M - \tilde{\boldsymbol{G}}_M^\top) + (\tilde{\boldsymbol{G}}_B - \tilde{\boldsymbol{G}}_B^\top)]\dot{\tilde{\boldsymbol{q}}}$$
$$+ [(\dot{\tilde{\boldsymbol{G}}}_M + \dot{\tilde{\boldsymbol{G}}}_B) + (\tilde{\boldsymbol{K}}_{M,U} - \tilde{\boldsymbol{K}}_{M,T}) + (\tilde{\boldsymbol{K}}_{B,U} - \tilde{\boldsymbol{K}}_{B,T})]\tilde{\boldsymbol{q}} = \boldsymbol{0} \tag{22}$$

where the combined matrices acting as the coefficients of $\ddot{\tilde{\boldsymbol{q}}}$, $\dot{\tilde{\boldsymbol{q}}}$, and $\tilde{\boldsymbol{q}}$ could be viewed as the system's equivalent mass, gyricity, and stiffness matrices, respectively. Note that the boom matrices are also placed in the augmented form of the same size as the

Table 1 Comparison of the results of Ref. [47] (using an extension of the present approach) and Ref. [67] (using FEM) to estimate the first 4 distinct modal frequencies of a fully deployed four-quadrant sail

Frequency	ω_1	ω_2	ω_4	ω_5
FEM [67] (rad/s)	0.0518	0.2085	0.3052	0.3678
From Ref. [47] (rad/s)	0.0533	0.2095	0.3100	0.3709

membrane ones by combining the two booms' matrices (together with a $\mathbf{0}$ partition corresponding to the membrane's generalized coordinates, $\boldsymbol{q}$) in block-diagonal form. For example, $\tilde{\boldsymbol{M}}_{\mathrm{B}} \triangleq \mathrm{blockdiag}\{\boldsymbol{M}_{\mathrm{B}}, \boldsymbol{M}_{\mathrm{B}}, 0_{n_{\mathrm{M}}\times n_{\mathrm{M}}}\}$, where $\boldsymbol{M}_{\mathrm{B}}$ is given by Eq. (18*a*) (transformed as described in Sec. 6.3), and so on for the other matrices. The general form of the matrices in Eq. (22) resembles that in Ref. [11] for their finite element formulation of beam-only deployment.

Lastly, highlighting another advantage of the transformed formulation is in order: the rate matrices $\dot{\tilde{\boldsymbol{M}}}$ and $\dot{\tilde{\boldsymbol{G}}}$ can be readily obtained by applying the chain rule to the external coefficients (functions of L and $\dot{L}$) of the transformed matrices in Sec. 6.3. In contrast, the use of Leibniz's integral rule (and evaluation of extra integrals) would have been necessary if the time-dependent integrands in Sec. 6.2 were to be used. As part of future work, when time-varying deployment rate is permitted, Eq. (22) should still hold, but the matrices in Eqs. (18*d*) and (20*d*) should be modified to account for acceleration-induced strain energies, and care must be taken not to omit $\mathrm{d}(\dot{L})/\mathrm{d}t$ when evaluating $\dot{\tilde{\boldsymbol{M}}}$ and $\dot{\tilde{\boldsymbol{G}}}$.

7 Numerical Simulations

This section presents some simulation results obtained for numerical examples. Section 7.1 attempts to validate the foundations of the formulation and its implementation in two ways: first, by discussing a comparison against the results in the literature for the modal analysis of a constant-length sail; and then, via dynamic simulations that minimize the membrane's effects and reproduce some of the past literature results on deploying beams. Section 7.2 uses a sample set of parameters that more closely resemble those appropriate for solar sails to simulate the system's deployment dynamics via numerical integration of the equations of motion in Sec. 6. Lastly, the vibration stability results of Sec. 5 are verified by comparing the results of the analytic derivation and numerical finite difference differentiation of the rate of change of energy. For all simulations, the number of modes used are $n_{\mathrm{B}} = 4$ for the booms and $n_{\mathrm{M}} = 16$ for the membrane, and the Newmark-Beta algorithm of Ref. [66] with $\beta = 1/2$ and a step-size of $\Delta t = 0.0001$ s is employed.

7.1 Model Validation. Before proceeding to deployment simulations with varying boom lengths, it is appropriate to assess the suitability of the presented formulation (such as the discretization in Eq. (15)) by considering the simpler problem of a constant-length sail. This was done in Ref. [47], which placed more emphasis on the dynamics of a complete sail and compared its constant-length results (using an extension of the formulation of this manuscript) against those obtained in Ref. [67] using FEM. Table 1 is reproduced from Ref. [47], and it compares the first four distinct eigenfrequencies obtained by both approaches, using $n_{\mathrm{B}} = 4$ and $n_{\mathrm{M}} = 16$ modes, $L(t) = L_0 = 50\sqrt{2}\,\mathrm{m}$, $\bar{\sigma} = 100\,\mathrm{kPa}$, and other physical parameters based on Ref. [68] (that will be revisited in Sec. 7.2). For a comparison of the mode shapes, the reader is referred to Refs. [47] and [67].

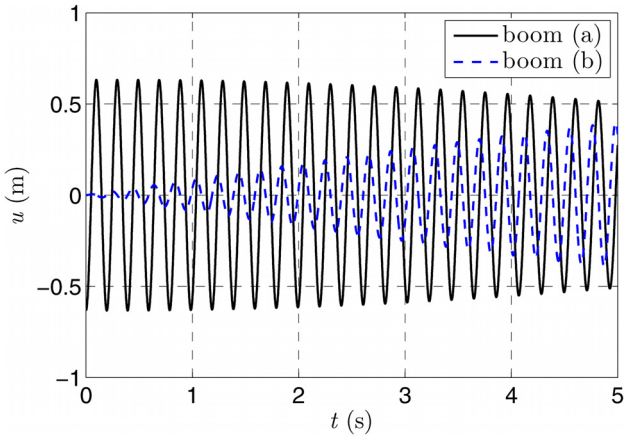

Fig. 3 Boom tip deflections during deployment with $\dot{L} = 0.1$ m/s

Next, based on the example considered in Refs. [16] and [69], the booms' parameters are then set to $\rho = 1\,\mathrm{kg/m}$ and $EI = 1.58 \times 10^8\ \mathrm{N{\cdot}m^2}$, and to minimize the effects of the membrane's motion on the booms' while still incorporating it in the simulation, its parameters are set to $\mu = 1 \times 10^{-3}\,\mathrm{kg/m^2}$ (negligibly small compared to the booms' density) and $\bar{\sigma} = 0$ (because of which the membrane's thickness and the booms' cross-sectional area are irrelevant). The initial conditions of boom (a) are set to $\boldsymbol{p}_{\mathrm{a}}(0.5) = [1\,0\,0\,0]^{\top}/\sqrt{L_0}$ and $\dot{\boldsymbol{p}}_{\mathrm{a}}(0.5) = \mathbf{0}_{4\times 1}$, while those of boom (b) are set to $\boldsymbol{p}_{\mathrm{b}}(0.5) = \mathbf{0}_{4\times 1}$ and $\dot{\boldsymbol{p}}_{\mathrm{b}}(0.5) = [1\,0\,0\,0]^{\top}/\sqrt{L_0}$, consistent with the two simulation cases of Refs. [16] and [69]. The membrane's deflection (along with its rate) relative to the booms' is set to zero via $\boldsymbol{q}(0.5) = \dot{\boldsymbol{q}}(0.5) = \mathbf{0}_{16\times 1}$.

Shown in Fig. 2 are the tip deflection histories obtained via backward and forward integration from $t_0 = 0.5$ s (both with profile $L = 108\ t$). As evident from the figures, despite the presence (however insignificant) of the membrane and the differences in the number of modes and numerical integration schemes used,

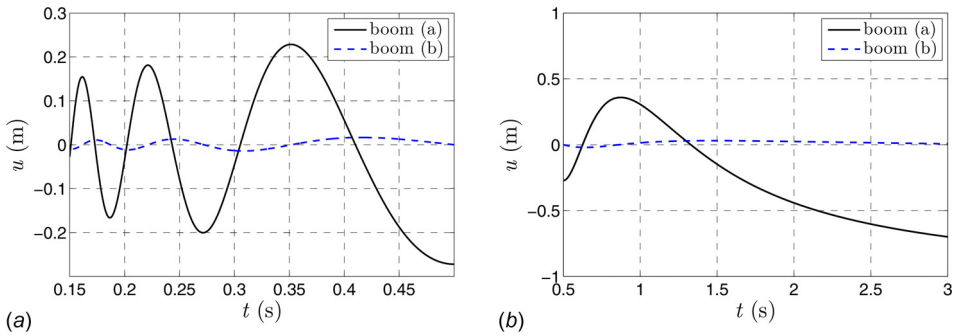

Fig. 2 Comparison of present deployment results (with negligible membrane effects) against beam-only deployment simulations of Refs. [16] and [69]: (*a*) backward and (*b*) forward simulation from $t_0 = 0.5$ s

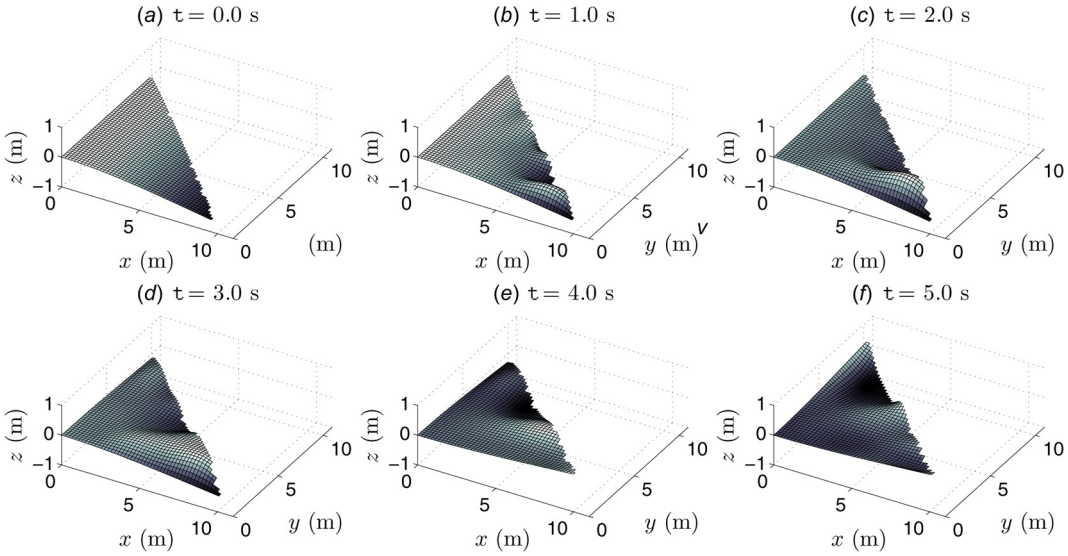

Fig. 4 Membrane deflections during deployment $\dot{L} = 0.1$ m/s at times (*a*) 0 s, (*b*) 1 s, (*c*) 2 s, (*d*) 3 s, (*e*) 4 s, and (*f*) 5 s

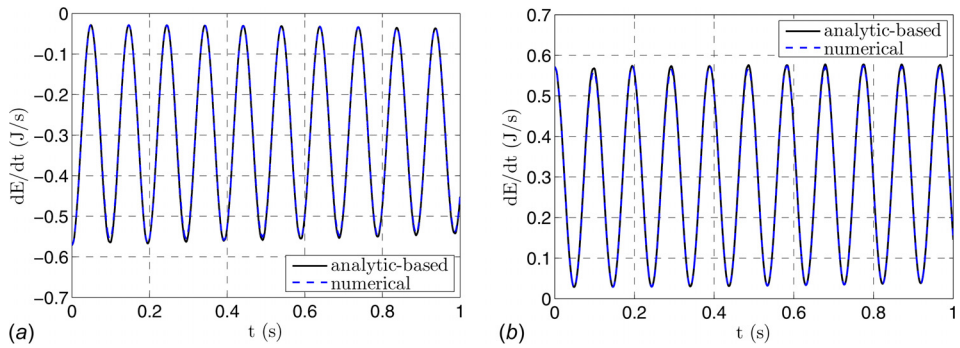

Fig. 5 Rate of change of vibration energy, $\dot{\mathscr{E}}_v$, during (*a*) $\dot{L} = 0.1$ m/s and (*b*) retraction with $\dot{L} = -0.1$ m/s

excellent agreement is obtained (other than with the second simulation case in Ref. [16] in the 0.5–3 s run, but as pointed out by Janković [69], their result appears to have been rescaled by a factor of 10 for that case).

7.2 Simulation of Dynamics. Based on the parameters used in Ref. [68] (halved when needed to account for the quadrant nature of the problem) which more closely resemble those to be expected for an actual sail, the booms' parameters are set to $\rho = 2.32 \times 10^{-2}$ kg/m, $EI = 2.31 \times 10^{4}$ N·m^2 (an order of magnitude higher than [68] to allow for shorter simulations), $A = 1.61 \times 10^{-5}$ m^2, and $L_0 = 10$ m; and the membrane's parameters are set to $\mu = 1.39 \times 10^{-2}$ kg/m^2, $\bar{\sigma} = 2 \times 10^{3}$ Pa, and $h = 1 \times 10^{-5}$ m. The initial conditions of boom (a) are set to $\boldsymbol{p}_a(0) = [1\,0\,0\,0]^\top/\sqrt{L_0}$ and $\dot{\boldsymbol{p}}_a(0) = \boldsymbol{0}_{4\times1}$, while those of boom (b) and the membrane are set to $\boldsymbol{p}_b(0) = \dot{\boldsymbol{p}}_b(0) = \boldsymbol{0}_{4\times1}$ and $\boldsymbol{q}(0) = \dot{\boldsymbol{q}}(0) = \boldsymbol{0}_{16\times1}$. In other words, only boom (a) is initially moved away from its neutral position and of interest are its vibrations during deployment and its motion's influence on the other two structural elements.

Shown in Fig. 3 are the tip deflection histories obtained from $t_0 = 0$ to $t_f = 5$ s with $\dot{L} = 0.1$ m/s, and presented in Fig. 4 are snapshots of the membrane's simulated motion in one-second intervals. As expected, because of the coupling provided by a now-significant membrane (that now has non-negligible mass and tension), boom (b) starts to vibrate during deployment as well, despite its initially neutral shape. Also noteworthy is the reduction in the amplitude of vibration of boom (a) during uniform extension: a different result from that in past literature on uniform deployment of a single beam (such as in Refs. [16] and [17]).

7.3 Dynamic Vibration Stability. Lastly, using the same sail quadrant parameters and initial conditions as those in Sec. 7.2, this section aims to numerically validate the analytic expression obtained in Sec. 5. To this end, the system's rates of change of vibration energy during extension ($\dot{L} = 0.1$ m/s) and retraction ($\dot{L} = -0.1$ m/s), plotted over time in Figs. 5(*a*) and 5(*b*), are obtained using the simulation results of Sec. 7.2 in two ways: via finite difference differentiation (dashed blue), $\dot{\mathscr{E}}_v(t) \approx [\mathscr{E}_v(t + \Delta t) \;\; -\mathscr{E}_v(t)]/\Delta t$; and using the analytic expression obtained in Eq. (14) (solid black). The agreement is excellent considering that the analytic procedure presented in this paper (detailed in Appendix B) uses the governing PDEs that are meant to exactly describe the motion subject to infinitely many modes, whereas the numerical simulation results in Sec. 7.2 are obtained using the discretized system in Eq. (22) with a finite number of modes. As expected, the energy rate remains negative for $\dot{L} > 0$ during extrusion, and positive for $\dot{L} < 0$ during retraction.

8 Conclusions

The uniform (constant-rate) deployment dynamics and stability of a coupled system consisting of two flexible Euler–Bernoulli booms and a thin membrane are studied, with the ultimate goal of facilitating the design and deployment of solar sails. Upon making

some simplifying assumptions and obtaining mathematical models that describe feasible stress and velocity distributions within the system, the equations of motion are obtained in both continuum and discretized forms. To this end, the applicability of Hamilton's principle is justified, and the variational approach of minimizing the time integral of the system's Lagrangian is used to obtain the coupled system of PDEs that describe the motion, along with their associated boundary conditions. Then, using time-varying basis functions based on the cantilevered beam and clamped membrane eigenfunctions, the deflections of the booms and the membrane are expanded in (hyperbolic) trigonometric series, while ensuring compatibility of the components' displacements along their connected edges by superimposing the clamped membrane deflections on those of the booms. The system matrices are obtained using the Euler–Lagrange equations, and subsequently transformed into forms with time-invariant integrals using a normalized coordinate system with fixed boundaries.

The stability of the coupled system of interest during its two-dimensional deployment is also studied from an energetics perspective. To this end, starting from the system's transverse vibration energy, analytic expressions are obtained for its rate of change. Upon evoking the stress and velocity fields considered for this problem, the total energy rate expression collapses down to an elegant form that is linear in deployment rate, allowing one to conclude vibration stability and instability (in the sense of boundedness of energy) during uniform extrusion and retraction, respectively. Lastly, numerical simulation results are provided to illustrate and validate the formulation of the model and the vibration stability analysis. Future work includes completion of current efforts on accounting for in-plane deflections, which would automatically refurbish the stress field hence eliminating the need for an Airy stress function; as well as allowing for time-varying deployment rate, which would require accounting for acceleration-induced strain energies and possibly a curved membrane free edge.

Acknowledgment

This research was supported by the Ontario Graduate Scholarship (OGS) program, jointly funded by the Province of Ontario and the University of Toronto.

Nomenclature

A = boom cross-sectional area
B = surface area of control volume
$\mathscr{E}$ = vibration energy
EI = boom bending stiffness
h = membrane thickness
L = boom length
$\mathscr{L}$ = Lagrangian
$\hat{\mathscr{L}}$ = Lagrangian areal density
$\hat{m}$ = mass density (generic)
n = number of discretized modes
N = force per unit length
$\hat{\boldsymbol{n}}$ = outward unit normal to control volume's boundary
$\vec{\boldsymbol{p}}$ = boom generalized coordinates
P = axial boom load
$\boldsymbol{q}$ = membrane generalized coordinates
$\tilde{\boldsymbol{q}}$ = augmented boom-membrane generalized coordinates
$\vec{\boldsymbol{r}}$ = mass element position
S = integration region on neutral plane
t = time
$\mathscr{T}$ = kinetic energy
u = boom out-of-plane deflection
$\mathscr{U}$ = potential energy
$\vec{\boldsymbol{v}}$ = mass element in-plane velocity
$\vec{\boldsymbol{V}}$ = control volume velocity
w = membrane (or boom) out-of-plane deflection

Greek Symbols

μ = membrane mass density
$\vec{\boldsymbol{\nu}}$ = mass element total velocity
ρ = boom mass density
σ = normal stress
$\bar{\sigma}$ = maximum initial boundary stress
τ = shear stress
ϕ = membrane basis function
Φ = airy stress function
ψ = boom basis function

Superscripts and Subscripts

$\hat{(\cdot)}$ = transformed (normalized) variable, or density
$\tilde{(\cdot)}$ = augmented (system-level) variable
$(\cdot)_{\mathrm{c}}$ = closed
$(\cdot)_{\mathrm{B,a}}, (\cdot)_{\mathrm{B,b}}$ = related to boom (a) or (b)
$(\cdot)_{\mathrm{M}}$ = related to membrane
$(\cdot)_{\mathrm{o}}$ = open
$(\cdot)_{,t}$ = temporal derivative with respect to t
$(\cdot)_{\mathrm{t}}$ = related to in-plane translation
$(\cdot)_{\mathrm{T}}$ = related to kinetic energy
$(\cdot)_{\mathrm{U}}$ = related to potential energy
$(\cdot)_{\mathrm{v}}$ = related to out-of-plane vibration
$(\cdot)_{,x}, (\cdot)_{,y}$ = spatial derivative with respect to x or y
$(\cdot)_{\mathrm{x}}, (\cdot)_{\mathrm{y}}$ = x- or y-component of a vector
$(\cdot)_{\mathrm{xx}}, (\cdot)_{\mathrm{yy}}$ = normal component along x or y
$(\cdot)_{\mathrm{yx}}, (\cdot)_{\mathrm{xy}}$ = shear component along x or y
$[(\cdot)]_{(x,y)}$ = evaluated at point (x, y)
$(\cdot)_0$ = initial value
$(\cdot)_{\mathrm{in}}$ = inside hub
$(\cdot)_{\mathrm{ex}}$ = exterior to hub

Operators

$\dot{(\cdot)}$ = temporal derivative with respect to t
$\mathrm{D}(\cdot)/\mathrm{D}t$ = first-order total (material) derivative
$\mathrm{D}^2(\cdot)/\mathrm{D}t^2$ = second-order total (material) derivative
$\vec{\nabla} \cdot (\cdot)$ = divergence of a vector field
$\delta(\cdot)$ = variation

Appendix A: Derivation of Governing Equations

Leibniz's integral rule and its two-dimensional analogue imply

$$\frac{\mathrm{d}}{\mathrm{d}t}\int_{0^+}^{L} f(x,y,t)\,dx = \int_{0^+}^{L} \frac{\partial}{\partial t} f(x,y,t)\,dx + \dot{L}\big[f(x,y,t)\big]_{y=L} \tag{A1a}$$

$$\frac{\mathrm{d}}{\mathrm{d}t}\int_{0^+}^{L}\int_{0^+}^{L-x} f(x,y,t)\,dy\,dx = \int_{0^+}^{L}\int_{0^+}^{L-x} \frac{\partial}{\partial t} f(x,y,t)\,dy\,dx + \dot{L}\int_{0^+}^{L}\big[f(x,y,t)\big]_{y=L-x}\,dx \tag{A1b}$$

where $f(x,y,t)$ is a generic scalar function. Noticing the Lagrangian densities, $\mathscr{L}$'s that form the integrands of Eqs. (8) and (9), depend only on the deflections' spatial and temporal derivatives, and following a procedure similar to Ref. [16] and using integration by parts, we have the following for the membrane-related constituents of the Lagrangian density variation:

$$\int_{t_1}^{t_2}\int_{0^+}^{L}\int_{0^+}^{L-x} \frac{\partial \hat{\mathscr{L}}_{\mathrm{M}}}{\partial w_{,x}}\delta w_{,x}\,dy\,dx\,dt = \int_{t_1}^{t_2}\int_{0^+}^{L}\left[\frac{\partial \hat{\mathscr{L}}_{\mathrm{M}}}{\partial w_{,x}}\delta w\right]_{x=0}^{x=L-y} dy\,dt - \int_{t_1}^{t_2}\int_{0^+}^{L}\int_{0^+}^{L-x} \frac{\partial}{\partial x}\frac{\partial \hat{\mathscr{L}}_{\mathrm{M}}}{\partial w_{,x}}\delta w\,dy\,dx\,dt \tag{A2a}$$

$$\int_{t_1}^{t_2}\int_{0^+}^{L}\int_{0^+}^{L-x}\frac{\partial\hat{\mathscr{L}}_{\mathrm{M}}}{\partial w_{,y}}\delta w_{,y}\,dy\,dx\,dt=\int_{t_1}^{t_2}\int_{0^+}^{L}\left[\frac{\partial\hat{\mathscr{L}}_{\mathrm{M}}}{\partial w_{,y}}\delta w\right]_{y=0}^{y=L-x}dx\,dt-\int_{t_1}^{t_2}\int_{0^+}^{L}\int_{0^+}^{L-x}\frac{\partial}{\partial y}\frac{\partial\hat{\mathscr{L}}_{\mathrm{M}}}{\partial w_{,y}}\delta w\,dy\,dx\,dt \tag{A2b}$$

$$\int_{t_1}^{t_2}\int_{0^+}^{L}\int_{0^+}^{L-x}\frac{\partial\hat{\mathscr{L}}_{\mathrm{M}}}{\partial w_{,t}}\delta w_{,t}\,dy\,dx\,dt=\int_{t_1}^{t_2}\int_{0^+}^{L}\left[\frac{\partial\hat{\mathscr{L}}_{\mathrm{M}}}{\partial w_{,t}}\delta w\right]_{y=L-x}dx\,dt-\int_{t_1}^{t_2}\int_{0^+}^{L}\int_{0^+}^{L-x}\frac{\partial}{\partial t}\frac{\partial\hat{\mathscr{L}}_{\mathrm{M}}}{\partial w_{,t}}\delta w\,dy\,dx\,dt+\left[\int_{0^+}^{L}\int_{0^+}^{L-x}\frac{\partial\hat{\mathscr{L}}_{\mathrm{M}}}{\partial w_{,t}}\delta w\,dy\,dx\right]_{t_1}^{t_2} \tag{A2c}$$

where Eq. (A1*b*) is used to arrive at Eq. (A2*c*). Analogous expressions corresponding to the booms' Lagrangians are available in the Appendix of Ref. [16]. Adding Eqs.(A2*a*) through (A2*c*) and the corresponding beam terms, and evoking Eq. (6) yields:

$$\begin{aligned}
0=&\int_{t_1}^{t_2}\int_{0^+}^{L}\int_{0^+}^{L-x}\left[-\frac{\partial}{\partial x}\frac{\partial\hat{\mathscr{L}}_{\mathrm{M}}}{\partial w_{,x}}-\frac{\partial}{\partial y}\frac{\partial\hat{\mathscr{L}}_{\mathrm{M}}}{\partial w_{,y}}-\frac{\partial}{\partial t}\frac{\partial\hat{\mathscr{L}}_{\mathrm{M}}}{\partial w_{,t}}\right]\delta w\,dy\,dx\,dt\\
&+\int_{t_1}^{t_2}\int_{0^+}^{L}\left[\left(\frac{\partial\hat{\mathscr{L}}_{\mathrm{M}}}{\partial w_{,x}}+\frac{\partial\hat{\mathscr{L}}_{\mathrm{M}}}{\partial w_{,y}}-\dot{L}\frac{\partial\hat{\mathscr{L}}_{\mathrm{M}}}{\partial w_{,t}}\right)\delta w\right]_{y=L-x}dx\,dt\\
&+\int_{t_1}^{t_2}\int_{0^+}^{L}\left[\left(-\frac{\partial}{\partial x}\frac{\partial\hat{\mathscr{L}}_{\mathrm{B,a}}}{\partial w_{,x}}+\frac{\partial^2}{\partial x^2}\frac{\partial\hat{\mathscr{L}}_{\mathrm{B,a}}}{\partial w_{,xx}}-\frac{\partial}{\partial t}\frac{\partial\hat{\mathscr{L}}_{\mathrm{B,a}}}{\partial w_{,t}}-\frac{\partial\hat{\mathscr{L}}_{\mathrm{M}}}{\partial w_{,y}}\right)\delta w\right]_{y=0}dx\,dt\\
&+\int_{t_1}^{t_2}\int_{0^+}^{L}\left[\left(-\frac{\partial}{\partial x}\frac{\partial\hat{\mathscr{L}}_{\mathrm{B,b}}}{\partial w_{,y}}+\frac{\partial^2}{\partial y^2}\frac{\partial\hat{\mathscr{L}}_{\mathrm{B,b}}}{\partial w_{,yy}}-\frac{\partial}{\partial t}\frac{\partial\hat{\mathscr{L}}_{\mathrm{B,b}}}{\partial w_{,t}}-\frac{\partial\hat{\mathscr{L}}_{\mathrm{M}}}{\partial w_{,x}}\right)\delta w\right]_{x=0}dy\,dt\\
&+\int_{t_1}^{t_2}\left[\left(\frac{\partial\hat{\mathscr{L}}_{\mathrm{B,a}}}{\partial w_{,x}}-\frac{\partial}{\partial x}\frac{\partial\hat{\mathscr{L}}_{\mathrm{B,a}}}{\partial w_{,xx}}-\dot{L}\frac{\partial\hat{\mathscr{L}}_{\mathrm{B,a}}}{\partial w_{,t}}\right)\delta w+\frac{\partial\hat{\mathscr{L}}_{\mathrm{B,a}}}{\partial w_{,xx}}\delta w_{,x}\right]_{(L,0)}dt\\
&+\int_{t_1}^{t_2}\left[\left(\frac{\partial\hat{\mathscr{L}}_{\mathrm{B,b}}}{\partial w_{,y}}-\frac{\partial}{\partial y}\frac{\partial\hat{\mathscr{L}}_{\mathrm{B,b}}}{\partial w_{,yy}}-\dot{L}\frac{\partial\hat{\mathscr{L}}_{\mathrm{B,b}}}{\partial w_{,t}}\right)\delta w+\frac{\partial\hat{\mathscr{L}}_{\mathrm{B,b}}}{\partial w_{,yy}}\delta w_{,y}\right]_{(0,L)}dt\\
&+\int_{t_1}^{t_2}\left[-\left(\frac{\partial\hat{\mathscr{L}}_{\mathrm{B,a}}}{\partial w_{,x}}-\frac{\partial}{\partial x}\frac{\partial\hat{\mathscr{L}}_{\mathrm{B,a}}}{\partial w_{,xx}}\right)\delta w+\frac{\partial\hat{\mathscr{L}}_{\mathrm{B,a}}}{\partial w_{,xx}}\delta w_{,x}\right]_{(0,0)}dt\\
&+\int_{t_1}^{t_2}\left[-\left(\frac{\partial\hat{\mathscr{L}}_{\mathrm{B,b}}}{\partial w_{,y}}-\frac{\partial}{\partial y}\frac{\partial\hat{\mathscr{L}}_{\mathrm{B,b}}}{\partial w_{,yy}}\right)\delta w+\frac{\partial\hat{\mathscr{L}}_{\mathrm{B,b}}}{\partial w_{,yy}}\delta w_{,y}\right]_{(0,0)}dt\\
&+\left[\int_{0^+}^{L}\int_{0^+}^{L-x}\frac{\partial\hat{\mathscr{L}}_{\mathrm{M}}}{\partial w_{,t}}\delta w\,dy\,dx+\int_{0^+}^{L}\left[\frac{\partial\hat{\mathscr{L}}_{\mathrm{B,a}}}{\partial w_{,t}}\delta w\right]_{y=0}dx+\int_{0^+}^{L}\left[\frac{\partial\hat{\mathscr{L}}_{\mathrm{B,b}}}{\partial w_{,t}}\delta w\right]_{x=0}dy\right]_{t=t_1}^{t=t_2}
\end{aligned} \tag{A3}$$

Requiring that $\delta w=0$ at $t=t_1$ and $t=t_2$ eliminates the last term, namely line 9. Setting $[\delta w=\delta w_{,x}=\delta w_{,y}\equiv 0]_{(0,0)}$ owing to the cantilevered nature of the booms eliminates lines 7 and 8. Requiring Eq. (A3) to hold for all admissible δw, $\delta w_{,x}$ and $\delta w_{,y}$, and hence setting their coefficients to zero yields: the booms' tip BCs from lines 5 and 6, the booms' governing equations from lines 3 and 4 (which could also be viewed as the membrane's attached edge BCs), the membrane's free edge BC from line 2, and the membrane's governing equation from line 1. Substituting $\hat{\mathscr{L}}$'s based on the integrands of Eqs. (8) and (9) into the equations that result from vanishing of the coefficients in Eq. (A3) eventually yields the governing equations in Eq. (10) and the natural BCs in Eq. (11) of Sec. 4.3.

Appendix B: Derivation of Vibration Energy Rate

The membrane's governing equation in Eqs. (10*a*) is rearranged as follows:

$$\begin{aligned}
\mu\left(w_{,tt}+\frac{\partial}{\partial t}(v_{\mathrm{x}}w_{,x})+\frac{\partial}{\partial t}(v_{\mathrm{y}}w_{,y})\right)=&-\mu\left(v_{\mathrm{x}}\frac{\partial}{\partial x}\frac{\mathrm{D}w}{\mathrm{D}t}+v_{\mathrm{y}}\frac{\partial}{\partial y}\frac{\mathrm{D}w}{\mathrm{D}t}+(v_{\mathrm{x},x}+v_{\mathrm{y},y})\frac{\mathrm{D}w}{\mathrm{D}t}\right)\\
&+\frac{\partial}{\partial x}(N_{\mathrm{xx}}w_{,x}+N_{\mathrm{xy}}w_{,y})+\frac{\partial}{\partial y}(N_{\mathrm{yy}}w_{,y}+N_{\mathrm{xy}}w_{,x})
\end{aligned} \tag{B1}$$

which is substituted back into Eq. (12*a*). Upon recognizing that $\mathrm{D}w/\mathrm{D}t\cdot\partial(\mathrm{D}w/\mathrm{D}t)/\partial x=1/2\cdot\partial(\mathrm{D}w/\mathrm{D}t)^2/\partial x$ (and similarly for y) and using the fundamental theorem of calculus and integration by parts, the first integral in Eq. (12*a*) can be rewritten in a form that cancels out the second integral in the same equation. Upon further manipulations involving the free edge BC of Eq. (11*a*) and using $[v_{\mathrm{x}}]_{x=0}=[v_{\mathrm{y}}]_{y=0}=0$ and $N_{\mathrm{xx}}=N_{\mathrm{yy}}=-N_{\mathrm{xy}}=\bar{N}$ from Eqs. (1) and (4), we arrive at

$$\dot{\mathscr{E}}_{\mathrm{M,v}} = -\frac{\mu}{2}\int_{0^+}^{L}\int_{0^+}^{L-x}(v_{\mathrm{x},x}+v_{\mathrm{y},y})(v_{\mathrm{x},x}+v_{\mathrm{y},y})\left(\frac{\mathrm{D}w}{\mathrm{D}t}\right)^2 dy\,dx - \int_{0^+}^{L}\left[\bar{N}\frac{\mathrm{D}w}{\mathrm{D}t}(w_{,y}-w_{,x})\right]_{y=0} dx - \int_{0^+}^{L}\left[\bar{N}\frac{\mathrm{D}w}{\mathrm{D}t}(w_{,x}-w_{,y})\right]_{x=0} dy$$
$$-\frac{1}{2}\int_{0^+}^{L}\left[\bar{N}(v_{\mathrm{x}}+v_{\mathrm{y}})(w_{,x}-w_{,y})^2\right]_{y=L-x} dx + \frac{1}{2}\int_{0^+}^{L}\left[\bar{N}v_{\mathrm{y}}^{\,0}(w_{,x}-w_{,y})^2\right]_{y=0} dx + \frac{1}{2}\int_{0^+}^{L}\left[\bar{N}v_{\mathrm{x}}^{\,0}(w_{,x}-w_{,y})^2\right]_{x=0} dy$$
$$+\frac{1}{2}\int_{0^+}^{L}\int_{0^+}^{L-x}\underbrace{\left[\bar{N}_{,x}v_{\mathrm{x}}+\bar{N}_{,y}v_{\mathrm{y}}-\bar{N}(v_{\mathrm{x},x}+v_{\mathrm{y},y})\right]}_{0}(w_{,x}-w_{,y})^2\,dy\,dx + \frac{\dot{L}}{2}\int_{0^+}^{L}\left[\bar{N}(w_{,x}-w_{,y})^2\right]_{y=L-x} dx \tag{B2}$$

where $v_{\mathrm{x}}+v_{\mathrm{y}}=\dot{L}$, $v_{\mathrm{x},x}+v_{\mathrm{y},y}=\dot{L}/(x+y)$, and $\bar{N}_{,x}=\bar{N}_{,y}=\bar{\sigma}h/L_0=\bar{N}/(x+y)$ are used. What remains of Eq. (B2) after these simplifications is given in Eq. (13*a*). Similarly, boom (a)'s governing equation in Eq. (10*b*) is rearranged as follows:

$$\left[\rho\left(w_{,tt}+\dot{L}w_{,xt}\right) = -\rho\left(\dot{L}w_{,xt}+\dot{L}^2w_{,xx}\right) - EIw_{,xxxx} + \frac{\partial}{\partial x}\left(P_{\mathrm{a}}w_{,x}\right) + \left(N_{\mathrm{yy}}w_{,y}+N_{\mathrm{xy}}w_{,x}\right)\right]_{y=0} \tag{B3}$$

which is substituted back into Eq. (12*b*). Upon expanding and performing integration by parts on the result, recognizing that $w_{,x}w_{,xx}=1/2\cdot\partial(w_{,x})^2/\partial x$ and $P_{\mathrm{a}}w_{,xx}w_{,xxx}=P_{\mathrm{a}}/2\cdot\partial(w_{,xx})^2/\partial x$, using integration by parts again and the fundamental theorem of calculus, and finally, using $N_{\mathrm{yy}}=-N_{\mathrm{xy}}=\bar{N}$ and evoking the tip and root BCs in Eq. (11) and its subsequent paragraph, we arrive at the following simplified form of Eq. (12*b*):

$$\dot{\mathscr{E}}_{\mathrm{B,a,v}} = \underbrace{\left[\frac{\dot{L}}{2}P_{\mathrm{a}}w_{,x}^2 - \frac{\dot{L}}{2}P_{\mathrm{a}}w_{,x}^2 + \frac{\dot{L}}{2}EIw_{,xx}^2\right]_{(L,0)}}_{0,\,\mathrm{BC}} - \underbrace{\left[-\frac{\dot{L}}{2}P_{\mathrm{a}}w_{,x}^2 + \frac{\dot{L}}{2}\mathrm{E}\mathrm{I}w_{,xx}^2\right]_{(0,0)}}_{0,\,\mathrm{BC}}$$
$$+\int_{0^+}^{L}\left[\frac{\dot{L}}{2}P_{\mathrm{a},x}w_{,x}^2\right]_{y=0} dx + \int_{0^+}^{L}\left[\bar{N}\frac{\mathrm{D}w}{\mathrm{D}t}(w_{,y}-w_{,x})\right]_{y=0} dx \tag{B4}$$

where, once again, the tip and root BCs in Eq. (11) and its subsequent paragraph are used. What remains of Eq. (B4) after these simplifications is given in Eq. (13*b*). Boom (*b*) will have similar expressions, but with x and y swapped.

References

[1] Lang, W. E., and Honeycutt, G. H., 1967, "Simulation of Deployment Dynamics of Spinning Spacecraft," National Aeronautics and Space Administration, Washington, DC, Report No. TN D-4074.

[2] Hedgepeth, J. M., 1970, "Dynamics of a Large Spin-Stiffened Deployable Paraboloidal Antenna," J. Spacecr. Rockets, **7**(9), pp. 1043–1048.

[3] Cloutier, G. J., 1968, "Dynamics of Deployment of Extendible Booms From Spinning Space Vehicles," J. Spacecr. Rockets, **5**(5), pp. 547–552.

[4] Cherchas, D. B., 1971, "Dynamics of Spin-Stabilized Satellites During Extension of Long Flexible Booms," J. Spacecr. Rockets, **8**(7), pp. 802–804.

[5] Hughes, P. C., 1972, "Dynamics of a Spin-Stabilized Satellite During Extension of Rigid Booms," C.A.S.I. Trans., **5**(1), pp. 11–14.

[6] Lips, K. W., and Modi, V. J., 1978, "Transient Attitude Dynamics of Satellites With Deploying Flexible Appendages," Acta Astronaut., **5**(10), pp. 797–815.

[7] Mote, C. D., Jr., 1972, "Dynamic Stability of Axially Moving Materials," Shock Vib. Dig., **4**(4), pp. 2–11.

[8] Wickert, J. A., and Mote, C. D., Jr., 1988, "Current Research on the Vibration and Stability of Axially-Moving Materials," Shock Vib. Dig., **20**(5), pp. 3–13.

[9] Wang, P. K. C., and Wei, J.-D., 1987, "Vibrations in a Moving Flexible Robot Arm," J. Sound Vib., **116**(1), pp. 149–160.

[10] Bergamaschi, S., and Sinopoli, A., 1983, "On the Flexural Vibrations of Arms With Variable Length: An Exact Solution," Mech. Res. Commun., **10**(6), pp. 341–344.

[11] Stylianou, M., and Tabarrok, B., 1994, "Finite Element Analysis of an Axially Moving Beam—Part I: Time Integration," J. Sound Vib., **178**(4), pp. 433–453.

[12] Behdinan, K., Stylianou, M. C., and Tabarrok, B., 1997, "Dynamics of Flexible Sliding Beams Non-linear Analysis—Part I: Formulation," J. Sound Vib., **208**(4), pp. 517–539.

[13] Wang, P. K. C., and Wei, J.-D., 1994, "Correction and Remarks on 'Vibrations in a Moving Flexible Robot Arm'," J. Sound Vib., **172**(3), pp. 413–414.

[14] Park, S., Yoo, H. H., and Chung, J., 2013, "Eulerian and Lagrangian Descriptions for the Vibration Analysis of a Deploying Beam," J. Mech. Sci. Technol., **27**(9), pp. 2637–2643.

[15] Leech, C. M., 1970, "The Dynamics of Beams Under the Influence of Convecting Inertial Forces," Ph.D. thesis, University of Toronto, Toronto, ON.

[16] Tabarrok, B., Leech, C. M., and Kim, Y. I., 1974, "On the Dynamics of an Axially Moving Beam," J. Franklin Inst., **297**(3), pp. 201–220.

[17] Wang, L. H., Hu, Z. D., Zhong, Z., and Ju, J. W., 2009, "Hamiltonian Dynamic Analysis of an Axially Translating Beam Featuring Time-Variant Velocity," Acta Mech., **206**(3–4), pp. 149–161.

[18] Wang, P. K. C., 1990, "Stabilization and Control of Distributed Systems With Time-Dependent Spatial Domains," J. Optim. Theory Appl., **65**(2), pp. 331–362.

[19] Stylianou, M., and Tabarrok, B., 1994, "Finite Element Analysis of an Axially Moving Beam—Part II: Stability Analysis," J. Sound Vib., **178**(4), pp. 455–481.

[20] Yuh, J., and Young, T., 1991, "Dynamic Modelling of an Axially Moving Beam in Rotation: Simulation and Experiment," ASME J. Dyn. Syst., Meas., Control, **113**(1), pp. 34–40.

[21] Niemi, J., and Pramila, A., 1987, "FEM-Analysis of Transverse Vibrations of an Axially Moving Membrane Immersed in Ideal Fluid," Int. J. Numer. Methods Eng., **24**(12), pp. 2301–2313.

[22] Koivurova, H., and Pramila, A., 1997, "Nonlinear Vibration of Axially Moving Membrane by Finite Element Method," Comput. Mech., **20**(6), pp. 573–581.

[23] Shin, C., Chung, J., and Kim, W., 2005, "Dynamic Characteristics of the Out-of-Plane Vibration for an Axially Moving Membrane," J. Sound Vib., **286**(4-5), pp. 1019–1031.

[24] Cherchas, P. C., and Gossain, D. M., 1974, "Dynamics of a Flexible Solar Array During Deployment From a Spinning Spacecraft," C.A.S.I. Trans., **7**(1), pp. 10–18.

[25] Cherchas, P. C., 1973, "Coupled Bending-Twisting Vibrations of a Single Boom Flexible Solar Array and Spacecraft," C.A.S.I. Trans., **6**(1), pp. 56–60.

[26] Hughes, P. C., 1976, "Deployment Dynamics of the Communications Technology Satellite—A Progress Report," ESRO Symposium on Dynamics and Control of Non-Rigid Spacecraft, pp. 335–340.

[27] Janković, M. S., 1979, "Deployment Dynamics of Flexible Spacecraft," Ph.D. thesis, University of Toronto, Toronto, ON.

[28] Hughes, P. C., and Garg, S. C., 1973, "Dynamics of Large Flexible Solar Arrays and Application to Spacecraft Attitude Control System Design," University of Toronto Institute for Aerospace Studies, Toronto, ON, Canada, Report No. 179.

[29] Shaker, F. J., 1976, "Free-Vibration Characteristics of a Large Split-Blanket Solar Array in a 1-g Field," National Aeronautics and Space Administration, Washington, DC, Report No. TN D83-7576.

[30] Weeks, G. E., 1986, "Dynamic Analysis of a Deployable Space Structure," J. Spacecr. Rockets, **23**(1), pp. 102–107.

[31] Seffen, K. A., and Pellegrino, S., 1999, "Deployment Dynamics of Tape Springs," Proc. R. Soc. London A: Math., Phys. Eng. Sci., **455**(1983), pp. 1003–1048.
[32] Walker, S. J. I., and Aglietti, G., 2004, "Study of the Dynamics of Three-dimensional Tape Spring Folds," AIAA J., **42**(4), pp. 850–856.
[33] Oberst, S., and Tuttle, S., 2018, "Nonlinear Dynamics of Thin-Walled Elastic Structures for Applications in Space," Mech. Syst. Signal Process., **110**, pp. 469–484.
[34] Shirasawa, Y., Mori, O., Miyazaki, Y., Sakamoto, H., Hasome, M., Okuizumi, N., Sawada, H., Furuya, H., Matsunaga, S., Natori, M., and Kawaguchi, J., 2011, " AIAA Paper No. 2011-1890.
[35] Zhao, J., Tian, Q., and Hu, H.-Y., 2013, "Deployment Dynamics of a Simplified Spinning IKAROS Solar Sail Via Absolute Coordinate Based Method," Acta Mech. Sin., **29**(1), pp. 132–142.
[36] Tian, Q., Zhao, J., Liu, C., and Zhou, C., 2015, "Dynamics of Space Deployable Structures," ASME Paper No. DETC2015-46159.
[37] Shabana, A. A., 1997, "Flexible Multibody Dynamics: Review of Past and Recent Developments," Multibody Syst. Dyn., **1**(2), pp. 189–222.
[38] Melnikov, V. M., and Koshelev, V. A., 1998, *Large Space Structures Formed by Centrifugal Forces*, Gordon and Breach Science Publishers, Philadelphia, PA.
[39] Miranker, W. L., 1960, "The Wave Equation in a Medium in Motion," IBM J. Res. Develop., **4**(1), pp. 36–42.
[40] Barakat, R., 1968, "Transverse Vibrations of a Moving Thin Rod," J. Acoust. Soc. Am., **43**(3), pp. 533–539.
[41] Wickert, J. A., and Mote, C. D., Jr., 1989, "On the Energetics of Axially Moving Continua," J. Acoust. Soc. Am., **85**(3), pp. 1365–1368.
[42] Zhu, W. D., and Ni, J., 2000, "Energetics and Stability of Translating Media With an Arbitrarily Varying Length," ASME J. Vib. Acoust., **122**(3), pp. 295–304.
[43] Yang, X.-D., Zhang, W., and Melnik, R. V. N., 2016, "Energetics and Invariants of Axially Deploying Beam With Uniform Velocity," AIAA J., **54**(7), pp. 2181–2187.
[44] Wickert, J. A., and Mote, C. D., Jr., 1990, "Classical Vibration Analysis of Axially Moving Continua," ASME J. Appl. Mech., **57**(3), pp. 738–744.
[45] Zhu, W. D., 2000, "Vibration and Stability of Time-Dependent Translating Media," Shock Vib. Dig., **32**(5), pp. 369–379.
[46] Lin, C. C., 1997, "Stability and Vibration Characteristics of Axially Moving Plates," Int. J. Solids Struct., **34**(24), pp. 3179–3190.
[47] Vatankhahghadim, B., and Damaren, C. J., 2018, "Solar Sail Deployment Dynamics," Fifth Joint International Conference on Multibody System Dynamics, Lisbon, Portugal, June 24–28.
[48] Zhang, L., and Zu, J. W., 1999, "Nonlinear Vibration of Parametrically Excited Viscoelastic Moving Belts, Part I: Dynamic Response," ASME J. Appl. Mech., **66**(2), pp. 396–402.
[49] Wickert, J. A., May 1992, "Non-Linear Vibration of a Travelling Tensioned Beam," Int. J. Non-Linear Mech., **27**(3), pp. 503–517.
[50] Behdinan, K., and Tabarrok, B., 1997, "Dynamics of Flexible Sliding Beams Non-Linear Analysis—Part II: Transient Response," J. Sound Vib., **208**(4), pp. 541–565.
[51] Zhang, L., and Zu, J. W., 1999, "Nonlinear Vibration of Parametrically Excited Viscoelastic Moving Belts, Part II: Stability Analysis," ASME J. Appl. Mech., **66**(2), pp. 403–409.
[52] Wu, K., and Zhu, W. D., 2014, "Parametric Instability in a Taut String With a Periodically Moving Boundary," ASME J. Appl. Mech., **81**(6), p. 061002.
[53] Öz, H. R., Pakdemirli, M., and Boyacı, H., 2001, "Non-Linear Vibrations and Stability of an Axially Moving Beam With Time-Dependent Velocity," Int. J. Non-Linear Mech., **36**(1), pp. 107–115.
[54] Ghayesh, M. H., and Amabili, M., 2013, "Steady-State Transverse Response of an Axially Moving Beam With Time-Dependent Axial Speed," Int. J. Non-Linear Mech., **49**, pp. 40–49.
[55] Wu, J., Shao, M., Wang, Y., Wu, Q., and Nie, Z., 2017, "Nonlinear Vibration Characteristics and Stability of the Printing Moving Membrane," J. Low Freq. Noise, Vib. Active Control, **36**(3), pp. 306–316.
[56] Jenkins, C. H., and Leonard, J. W., 1991, "Nonlinear Dynamic Response of Membranes: State of the Art," ASME Appl. Mech. Rev., **44**(7), pp. 319–328.
[57] Jenkins, C. H., 1996, "Nonlinear Dynamic Response of Membranes: State of the Art - Update," ASME Appl. Mech. Rev., **49**(10S), pp. S41–S48.
[58] Shin, C., Chung, J., and Yoo, H. H., 2006, "Dynamic Responses of the In-Plane and Out-of-Plane Vibrations for an Axially Moving Membrane," J. Sound Vib., **297**(3–5), pp. 794–809.
[59] Li, Q., Ma, X., and Wang, T., 2011, "Reduced Model for Flexible Solar Sail Dynamics," J. Spacecr. Rockets, **48**(3), pp. 446–453.
[60] Timoshenko, S., 1934, *Theory of Elasticity*, McGraw-Hill, New York.
[61] Lanczos, C., 1986, *The Variational Principles of Mechanics*, Dover Publications, Mineola, NY, Chap. 4.
[62] McIver, D. B., 1973, "Hamilton's Principle for Systems of Changing Mass," J. Eng. Math., **7**(3), pp. 249–261.
[63] Timoshenko, S., and Woinowsky-Krieger, S., 1940, *Theory of Plates and Shells*, McGraw-Hill, New York.
[64] Kane, T. R., Likins, P. W., and Levinson, D. A., 1983, *Spacecraft Dynamics*, McGraw-Hill, New York.
[65] Shames, I. H., and Dym, C. L., 1985, *Energy and Finite Element Methods in Structural Mechanics*, Hemisphere Publishing, Philadelphia, PA, Chap. 3-D.
[66] Newmark, N. M., 1959, "A Method of Computation for Structural Dynamics," ASCE J. Eng. Mech. Div., **85**(3), pp. 67–94.
[67] Hassanpour, S., and Damaren, C. J., 2018, "Linear Structural Dynamics and Modal Cost Analysis for a Solar Sail," AIAA Paper No. 2018-1434.
[68] Choi, M., 2015, "Flexible Dynamics and Attitude Control of a Square Solar Sail," Ph.D. thesis, University of Toronto, Toronto, ON.
[69] Janković, M. S., 1976, "Lateral Vibrations of an Extending Rod," University of Toronto Institute for Aerospace Studies, Toronto, ON, Technical Report No. 202.